Received: 30 April 2024 | Revised: 26 October 2024 | Accepted: 8 December 2024

DOI: 10.1002/suco.202400577

ARTICLE

fib CEB-FIP WILEY

A fiber-based deterioration modeling framework for reinforced concrete structures subject to spatially non-uniform corrosion patterns described by limited information

Davide Bernardini | **Daniela Ruta** | **Paolo Di Re** | **Achille Paolone**

Department of Structural and Geotechnical Engineering, University of Rome Sapienza, Rome, Italy

Correspondence
Davide Bernardini, Department of Structural and Geotechnical Engineering, University of Rome Sapienza, Rome, Italy.
Email: davide.bernardini@uniroma1.it

Abstract

Reinforced concrete structures are often subject to significantly non-uniform corrosion patterns. In real situations, the information available about deterioration is incomplete and sometimes is reduced to qualitative judgments formulated by inspectors based on in-situ surveys. This work proposes a practice-oriented fiber-based modeling approach capable to model arbitrary spatial distributions of corrosion characterized by limited information. The approach is based on the partition of the structure into pieces, regions and zones and by the use of degradation laws for material parameters. Local and global deterioration scales are introduced to facilitate consistent specification of material parameters on the basis of qualitative judgments. The penetration of deterioration beyond the exposed surfaces is modeled by the concepts of exposition zone and deterioration attenuation laws. The approach has been implemented in a macroelement of arbitrarily corroded beam-column in OpenseesPy and validated by comparison with 16 experimental tests of columns with different section types, corrosion intensities, axial load and confinement levels. Results show that strength and ultimate drift can be predicted with remarkable accuracy.

KEYWORDS

aging structures, bridge piers, corrosion, degradation laws, nonlinear modeling, reinforced concrete

1 | INTRODUCTION

Steel corrosion in reinforced concrete (RC) elements can produce significant degradation of structural performances and, in many cases, takes place in a strongly non-uniform way (Figure 1).

Engineering practice often requires nonlinear modeling of large RC elements subject to complex corrosion patterns using only limited knowledge gathered from in-situ surveys. This happens, for example, during the assessment of the seismic performances of aging bridges with corroded piers which may have complex

FIGURE 1 Examples of RC bridge piers subject to spatially non-uniform corrosion.

geometry, reinforcement layout and deterioration patterns.

Generally speaking, the detailed modeling of the effects of corrosion on RC structures requires a multi-disciplinary and multi-physics approach. For elements with a few bars subject to simple corrosion patterns, 2D or 3D models taking into account fine details can be developed with considerable accuracy (see e.g., references [1,2]). However, in practical contexts, 2D or 3D models are unfeasible due to their computational cost, whereas 1D fiber-based (FB) models offer a good compromise between modeling detail and computational cost.

The FB approach has been applied to RC structures with simple corrosion patterns by letting material properties of the fibers to depend on deterioration intensity via suitable degradation laws (see e.g., references [3,4] for a state of the art review). Although this idea is fruitful and straightforward, its application to real structures subject to complex deterioration scenarios poses specific challenges:

- a complete characterization of the deterioration would require the knowledge of the corrosion intensity and morphology for each bar and each stirrup as well as the cracking state of cover and core concrete. In practical cases, this information is not available and the specification of consistent sets of material parameters becomes a non-trivial task;
- in severe corrosion states, deterioration penetrates beyond the external surface (Figure 2);
- due to non-uniform corrosion of stirrups, confinement in the core of large sections can be reduced differently in the various parts of the section;

FIGURE 2 Examples of deterioration penetration beyond external surface, sometimes observed under severe corrosion.

- several degradation laws for the materials are available in the literature (see e.g., reference [5] for a review related to steel), each one based on different tests with specific features. In practical cases various corrosion types can be found and the choice of specific laws is not trivial.

A practically useful modeling approach should address the above issues while being implementable on the basis of the limited information usually available, namely in-situ surveys carried out by standard inspectors. This work proposes a modeling approach which defines an algorithm (Figure 10) for the assignment of material parameters to all fibers consistent with the deterioration state of the external surface, taking into account the penetration of deterioration within the structure and the effects of partial stirrups corrosion. This extends and completes in several respects the preliminary versions presented in references [6,7].

A new set of degradation laws for steel is proposed in Section 4.1.1 based on the statistical analysis of 17 existing laws calibrated on a total of 898 experimental tests. The new laws have been conceived to facilitate its application to cases of limited knowledge of the corrosion intensity and morphology. Degradation laws for concrete are discussed in Section 4.1.2. Issues related to the modeling of deteriorated confined concrete are discussed in Section 4.1.3. Deterioration levels of the various zones of the structure are defined by qualitative scales (Section 4.3) which are translated into quantitative ranges of material parameters by inverting the degradation laws (Section 4.2). Deterioration levels of the external surface can be assigned by using the limited information available from standard inspections. The proposed approach has been concretely implemented in OpenseesPy in the form of a macroelement of arbitrarily corroded beam-column that can be combined at will to model not only single-columns piers but also framed piers or more complex structures composed assemblies of 1D elements (Section 6). Finally, Section 7 presents a validation of the modeling approach against experimental results.

This research originated within the project PRESID-EST promoted by the Italian Ministry of Infrastructures with the involvement of two universities (Rome Sapienza and Basilicata) and funded by the main company managing Italian highways (Autostrade per l'Italia).[8] In this context, a large database of nearly 3000 real piers has been used to set up the proposed approach.

2 | MODELING DETERIORATED SECTIONS

In presence of non-uniform corrosion, fibers parameters depend on deterioration and vary all over the structure. To implement this fact, it is useful to introduce the following terminology.

A *region*, is a part of a section that can be discretized into several fibers with the same uniaxial constitutive law. Longitudinal steel (LS) regions, located along rebars alignments, are composed by one fiber per bar. Unconfined concrete (UC) and confined concrete (CC) regions, located in the cover and in the confined core, are discretized into several fibers. Whereas for plain structures one region per material usually suffices, corroded sections may require several regions of the same material with different levels of deterioration. Partition into regions depends therefore on the level of detail in the modeling of sectional corrosion pattern. Figure 3 shows an example of partition of a rectangular hollow section into regions that allows the modeler to specify different deterioration

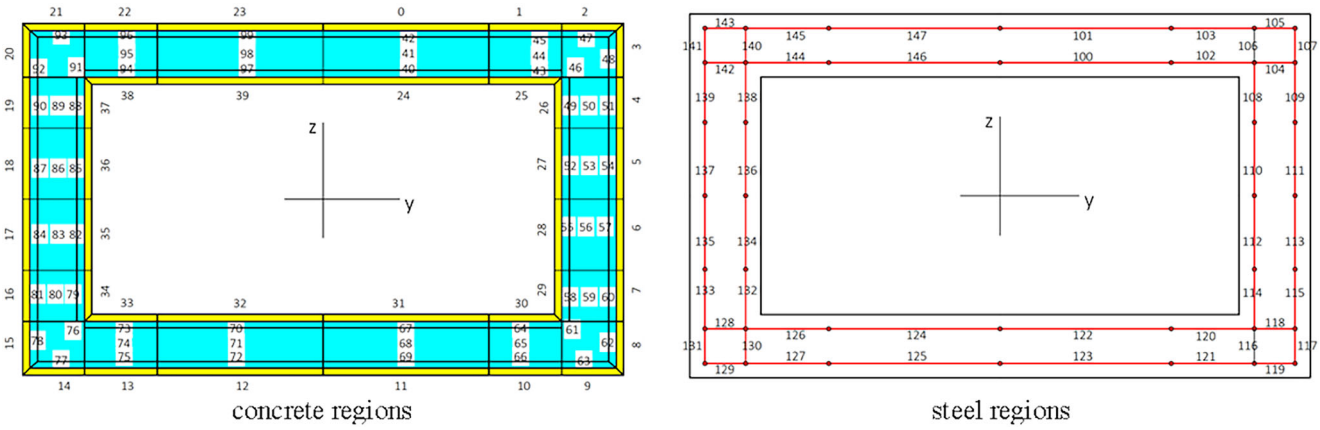

FIGURE 3 Illustrative example of a rectangular hollow section partitioned into: 40 UC regions (yellow), 60 CC regions (cyan) and 47 LS regions (red).

levels on the angles and on each quarter of each wall. Finer or coarser descriptions of deterioration can be implemented by modifying the partitions into regions.

To facilitate the consistent assignment of material parameters, regions can be grouped according to various criteria. A *zone* is a group of regions sharing some property or condition (e.g., confinement level or exposition to corrosion).

2.1 | Uniform confinement zones

CC regions are peculiar since confinement is intrinsically a non-local phenomenon. The lateral pressure on a region is the result of the combined action of legs of stirrups, spirals or ties that may be located far from the region itself. This aspect is seldom relevant for plain sections, but becomes important for large corroded sections since corrosion of a part of a stirrup may lead to the reduction of confinement in several CC regions.

To model this aspect, CC regions are grouped into *Uniform Confinement Zones* (UCZ) assumed to be confined by a common perimetral stirrup and eventually further internal reinforcement. To illustrate the idea, Figure 4 shows the partition of the section of Figure 3 in 12 uniform confinement zones. For example, CZ1 contains 6 CC regions assumed to be confined by the same perimetral stirrups. The utility to group CC regions in this way is related to the possibility to specify different confinement reductions in presence of stirrups corrosion. Specifically, if one or both exposed legs of the perimetral stirrup of CZ1 is corroded the confinement of all CC regions within CZ1 is reduced accordingly. Partition of the section into UCZ depends therefore both on stirrups layout and on the desired level of detail in corrosion modeling.

2.2 | Exposition zones

As discussed in the Introduction, deterioration can penetrate beyond the external surface, especially in presence of severe corrosion levels (Figure 2). To model this phenomenon it is useful to group regions into layers parallel to the external surface, in a way reminiscent of the stratification of the onion skin.

An *exposition zone* is a part of a section, which, for the purpose of modeling, can be assumed to be exposed to a similar influx of aggressive agents and, consequently, is expected to exhibit a similar level of deterioration.

Steel corrosion is activated when aggressive agents (CO_2, chlorides) reach the bars, trigger depassivation and progresses due to influx of oxygen and water. Depending on the corrosive agents environmental abundance and concrete permeability, deterioration can be present not only on the most superficial part but also in the interior of the element. Assuming that penetration of aggressive agents takes place orthogonally to the lateral surface, exposition zones can be organized as follows:

- an *exposed layer* (EL) directly exposed to environmental actions, typically coincident with the cover region;
- a sequence of *superficial layers* (SL), potentially subject to influx of aggressive agents and non-negligible deterioration ordered according to the depth in the stratification. The number of layers and their width is a

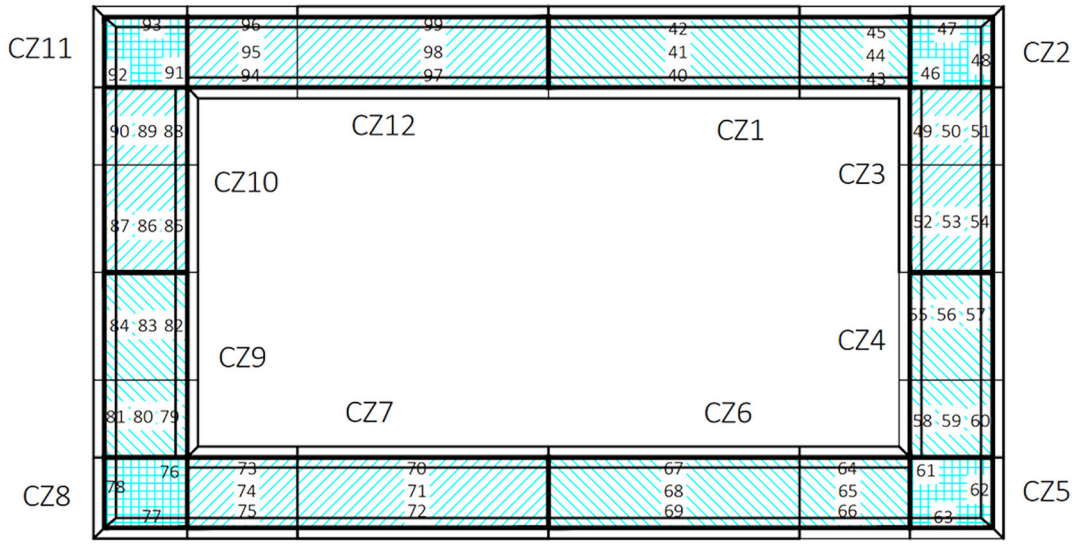

FIGURE 4 Partition of CC regions into UCZ for the section in Figure 3.

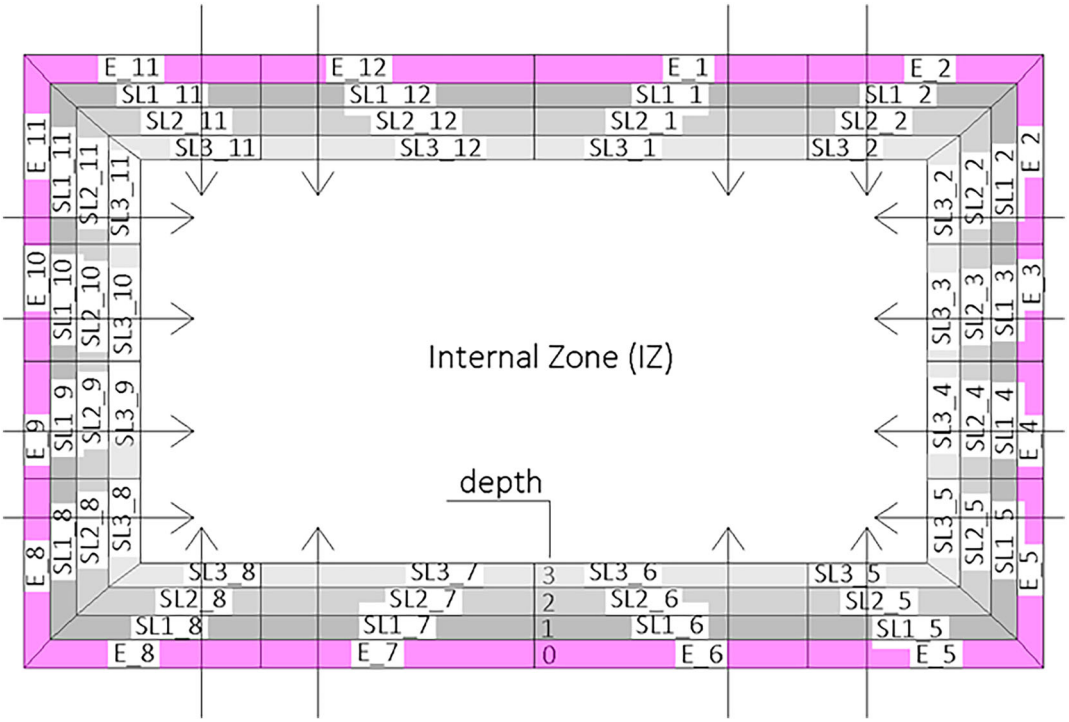

FIGURE 5 Illustrative example of deterioration penetration pattern for a solid rectangular section. Arrows indicate aggression paths.

modeling choice that can be made taking into account aggressivity of the environment, concrete permeability, cracking state. A stratification with a width of a few cover depths usually suffices to describe most deterioration scenarios (Figure 5);
- an *internal zone* where penetration of aggressive agents is not enough to produce significant deterioration.

Environmental actions can vary over the exposed surface. For example, in bridge piers, lateral parts may be more subject to water percolation than those protected by the superstructure. In other cases, external sides may be protected by pier caps whereas percolation may occur through unsealed joints. To model this effect, external and superficial layers are partitioned into *aggression paths* by assigning to each region three *exposition parameters*:

- the type of layer to which the region belongs (exposed, superficial or internal);
- the *depth* of the layer within the stratification;
- the region of the adjacent less superficial layer from which it can receive aggressive agents.

To illustrate the idea, Figure 5 shows an example of a solid rectangular section partitioned into: one external layer (magenta), three superficial layers (gray) and the remaining internal zone (white). Layers are partitioned in 12 aggression paths indicated by arrows. For example, zones SL1_2, SL2_2, SL3_2 can receive aggressive agents from zone E_2. Layers SL_1, SL_2, SL_3 have respective depth levels 1, 2, 3.

Concerning CC regions, after the definition of the exposition layers, for each UCZ all the exposed layers through which the legs of the perimetral stirrups passes are recorded. For example, if the rectangular section in Figure 5 has a single UCZ, its perimetral stirrup passes through all the 12 zones of the EL, therefore corrosion in any one of them can influence confinement in the whole section.

3 | DETERIORATION SCENARIOS

Once the various sections and the corrosion patterns have been identified and modeled, the model of the structure can be built by assembling the various pieces.

A *piece* is a component of the structure that can be discretized into one or more groups of finite elements with the same cross-section (*deformable parts*). More than one piece is required to model, for example, multiple-columns piers or framed structures. More than one part is required in presence of changes in concrete geometry, reinforcement layout or corrosion patterns.

Summarizing, a deterioration *scenario* for a corroded structure is defined by:

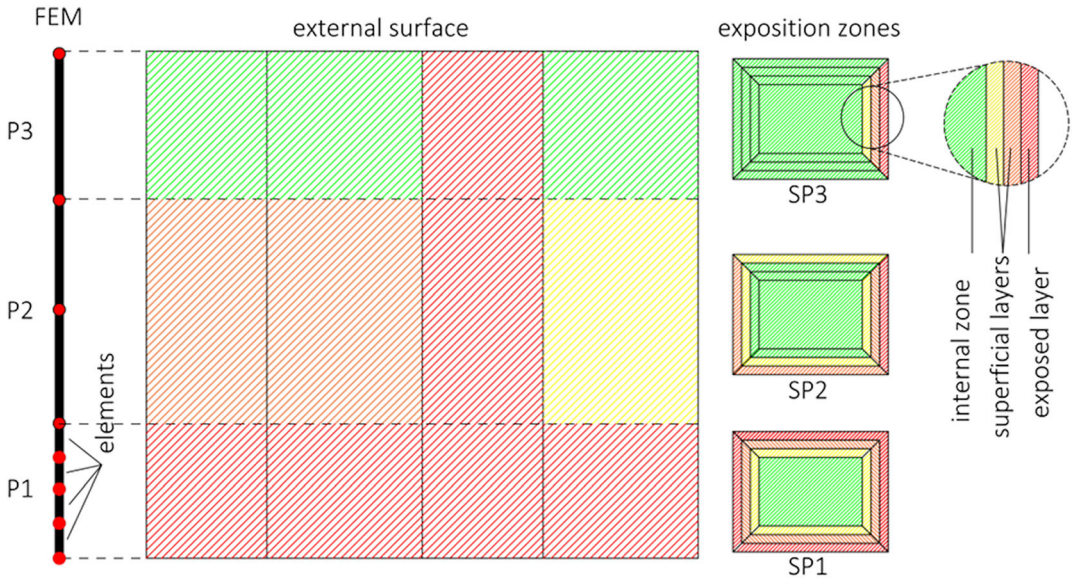

FIGURE 6 Illustrative example of a deterioration scenario for a single-column pier with solid rectangular section.

- a partition of the structure into pieces and parts specifying how deteriorated sections are distributed (*deterioration elevation pattern*);
- a partition of the section of each part into exposition zones specifying how susceptible to deterioration are the various parts of the section (*deterioration penetration pattern*);
- the assignment of suitable corrosion intensity measures to all the regions (*deterioration intensity distribution*).

To illustrate the idea, Figure 6 shows an example of a single-column pier modeled as a single piece with three deformable parts composed by a different number of finite elements. Each part has a sectional pattern determined by three layers. Colors indicate different deterioration intensities, to be defined as indicated in Section 4.3.

4 | MEASURES OF DETERIORATION INTENSITY

To complete the definition of a deterioration scenario it is necessary to define deterioration intensity distributions.

If corrosion intensity and morphology would be known in each bar and the cracking state would be known for all concrete regions then it would possible to assign material parameters to all fibers without further considerations. However, if corrosion patterns are known only through limited information, the assignment of parameters should follow from qualitative judgments related to the progression of corrosion. Of course, this cannot be made without strong and drastic approximations. To this end, we propose in Section 4.3, a global deterioration scale for zones parameterized by synthetic judgments which are translated into quantitative ranges of local deterioration intensities for regions defined in Sections 4.1 and 4.2.

4.1 | Local deterioration intensity for regions

Regions of the same material may have different parameters since they may differently deteriorated and the influence of corrosion can be evaluated by means of *degradation laws*

$$X_D = f(X_P; d) \tag{1}$$

where X_P and X_D are the values assumed by the parameter X in plain and deteriorated conditions, and d indicates *Deterioration Intensity Measures* (DIM) parameterizing corrosion intensity. Expressions like (1) are common in the literature and are typically obtained from statistical analysis of experimental datasets, where the function f often takes the form of a linear or exponential regression.

In principle, the proposed modeling approach can be applied with any degradation laws. However, since the explicit definition of a global deterioration scale (Section 4.3) depends on the degradation laws used for the materials, in the next sections, some specific choices are presented for later use.

4.1.1 | Degradation laws for steel

Steel corrosion can produce significant morphological changes of bars[9] and its intensity can be parameterized by different measures, the more global one being *mass loss*:

$$\psi = \frac{m_P - m_D}{m_P} \tag{2}$$

where m_P, m_D denote mass before and after corrosion. Alternatively, corrosion can be parameterized by residual area, variable along the bar according to: $A_D(x) = \overline{A_D} + \Delta(x)$ where $\overline{A_D}$ is the average corroded area and Δ is fluctuation about mean value. Two common area-based measures are:

$$\begin{aligned} \eta &= \frac{A_P - \overline{A_D}}{A_P} (\text{average area loss}),\ \eta_{cr} \\ &= \frac{A_P - A_{cr}}{A_P} (\text{maximum area loss}) \end{aligned} \tag{3}$$

where A_P is the uncorroded area and $A_{cr} = \min_x A_D(x)$. In some cases, it is useful to describe corrosion in terms of diameter, to be interpreted heuristically since cross-sections usually loose their circularity. *Residual effective diameter* ϕ_D can be defined as the diameter of a circular section with area $\overline{A_D}$ and used to evaluate:

$$\eta_\phi = \frac{\phi_P - \phi_D}{\phi_P} \text{ (average diameter loss)} \tag{4}$$

Corrosion can be parameterized also by *attack penetration* p corresponding to a residual diameter $\phi_D = \phi_P - \alpha p$, where $\alpha = 2$ corresponds to the symmetric attack of uniform corrosion, while bigger values, up to $\alpha = 8$, correspond to more and more localized pits. The various measures are related by:

$$\psi = \eta - R,\ \ \eta = 1 - (1 - \eta_\phi)^2,\ \ \eta_\phi = \frac{\alpha p}{\phi_P} \tag{5}$$

where $R = \int_0^L \Delta(x)dx / A_P L = \Delta_{med}/A_P$ measures non-uniformity of corrosion. It turns out that mass loss and average area loss coincide only if area fluctuations have zero average. Concerning maximum area loss, Li et al.[10] found a linear correlation with mass loss $\eta_{cr} = 1.66\psi$.

Several degradation laws have been proposed in the literature for artificial and natural corrosion.[5] It is generally agreed that the parameters more influenced by corrosion are: yield stress f_{sy}, peak stress f_{su}, ultimate strain ε_{su} and that degradation laws can be put in the form:

$$\begin{aligned} f_{sy,D} &= \left(K_{f_{sy}}\right) f_{sy,P} \\ f_{su,D} &= \left(K_{f_{su}}\right) f_{su,P} \\ \varepsilon_{su,D} &= \left(K_{\varepsilon_{su}}\right) \varepsilon_{su,P} \end{aligned} \tag{6}$$

Only in a few cases a light dependence of elastic modulus has been observed,[11] but since there is no agreement, this is disregarded hereafter.

An important point related to degradation laws for steel is the very definition of stress. Effective stresses defined in terms of critical area A_{cr} exhibit much smaller degradation than nominal stresses defined with respect to uncorroded area A_P.[9] As pointed out, for example in reference [12], the degradation of effective stresses can be attributed both to local concentrations of microstresses and to the differences between the microstructure of the external shell and the internal part. Since determination of A_{cr} may be difficult in practical cases, for large-scale modeling, nominal stresses are used in conjunction with fibers having uncorroded area.

Although some authors proposed degradation laws in terms of η and η_{cr},[9] mass loss is the most common DIM. Besides its easier determination, ψ has the drawback that it cannot distinguish between uniform and pitting corrosion. To mitigate this issue, many authors proposed different laws for the two types of corrosion.

Concerning the functional form of the law, there is a general agreement on linear dependence of stresses on mass loss, whereas for ultimate strain both linear and exponential laws have been proposed (Table 1).

Table 2 summarizes the parameters corresponding to 17 laws available in the literature.

As it is evident from the table, each law has been derived under specific conditions and has a different range of applicability. In the modeling of real structures, all types of corrosion can be found and therefore the choice of one law in favor of others can be subjectively biased.

Table 3 shows mean values and coefficients of variation for the laws in Table 2. It turns out that laws for uniform corrosion have smaller dispersion than pitting and that linear laws for ε_{su} have a very large dispersion with values sometimes close to 100%.

Having in mind applications to a variety of different contexts, instead of choosing a specific law, we propose

TABLE 1 Functional form of degradation laws for steel.

	$K_{f_{sy}}$	$K_{f_{su}}$	$K_{\varepsilon_{su}}$
Linear	$1-\alpha_1\psi$	$1-\alpha_2\psi$	$1-\alpha_3\psi$
Exponential	-	-	$e^{-\alpha_4\psi}$

TABLE 2 Summary of the steel degradation laws selected for the statistical analysis.

	Tests		Law coefficients				Corrosion					
Source	**Number**	ψ_{max}	α_1	α_2	α_3	α_4	**Type**	**Cause**	**Bars**	**Process**	**Current**	**Method**
Imperatore et al.[12]	-	40.0	1.996	1.864	5.470	-	Pitting	Variable	-	-	-	-
Lee and Cho[13]	64	35.0	1.980	1.570	-	2.590	Pitting	Artif.	In concrete	Wet and dry cycles	-	High temperature
Liu et al.[9]	53	32.5	1.516	1.533	5.510	-	Pitting	Artif.	In concrete	Current	0.3 mA/cm^2	Partially-immersed
Lu et al.[14]	31	5.8	1.950	2.310	-	-	Pitting	Artif.	In cracked concrete	Wet and dry cycles	-	4 years
Ou et al.[11]	18	82.4	1.230	1.150	-	1.250	Pitting	Natural	In concrete	-	-	30 yo
Vanama and Ramakrishnan[15]	38	79.6	1.220	1.194	2.923	-	Pitting	Natural	In concrete	-	-	54 yo
Xia et al.[16]	212	15.0	2.100	2.100	-	0.800	Pitting	Artif.	In concrete	Current	2 mA/cm^2	Wet sponge
Zhang et al.[17]	45	31.2	1.120	1.360	-	-	Pitting	Natural	In concrete	-	-	>30 yo
Du et al.[18]	108	25.0	1.400	1.400	-	2.900	Pitting	Artif.	Bare and in concrete	Current	0.5–2 mA/cm^2	Immersed
Imperatore et al.[12]	14	53.2	1.510	1.382	2.771	-	Unif.	Artif.	Bare	Current	0.1 mA	Immersed
Imperatore et al.[12]	66	36.0	1.435	1.253	2.050	-	Unif.	Artif.	Bare	Current	0.1 mA	Immersed
Lee and Cho[13]	34	33.0	1.240	1.070	-	1.950	Unif.	Artif.	In concrete	Current	n.s.	Immersed
Ou et al.[11]	29	31.4	1.270	1.160	-	2.810	Unif.	Artif.	In concrete	Current	0.6 mA/cm^2	Immersed
Sun et al.[19]	30	12.0	1.100	1.300	-	6.964	Unif.	Artif.	Bare	Current	0.4 mA/cm^2	Wet sponge
Vanama and Ramakrishnan[15]	15	47.6	1.363	1.280	2.923	-	Unif.	Artif.	Bare	Current	4.4 mA/cm^2	Partially-immersed
Xia et al.[16]	120	58.0	1.200	1.200	-	0.200	Unif.	Artif.	Bare	Current	2 mA/cm^2	Wet sponge
Zhang et al.[17]	21	39.7	1.100	1.220	-	-	Unif.	Artif.	In concrete	Current	0.1 mA/cm^2	Partially-immersed
Total number of samples	898											

	α_1	α_2	α_3	α_4	
All tests	1.42	1.41	3.24	2.43	Mean
	22.6%	24.4%	40.9%	85.4%	Coeff. var.
Uniform corrosion	1.28	1.23	2.58	2.98	Mean
	11.7%	7.7%	18.1%	96.2%	Coeff. var.
Pitting corrosion	1.61	1.61	4.63	1.77	Mean
	24.3%	25.0%	32.0%	52.8%	Coeff. var.

TABLE 3 Statistics of degradation laws in Table 2.

TABLE 4 Proposed degradation laws for steel.

	α_1	α_2	α_3
Uniform corrosion	1.277	1.233	2.581
Pitting corrosion			
Mild	1.220	1.207	3.152
Average	1.612	1.609	4.634
Strong	2.005	2.011	6.116

new degradation laws determined from the above statistical analysis. Due to the inherently different dispersion, we propose: to discard linear law for ε_{su}, a single law for uniform corrosion and a triple law for pitting. Denoting μ_i, σ_i, mean and standard deviation for the coefficient α_i, the laws for mild, average and strong pitting are defined by $\mu_i - \sigma_i$, σ_i and $\mu_i + \sigma_i$, while law for uniform corrosion corresponds to μ_i.

The new law based on Formulas (6), expressions in Table 1 and coefficients in Table 4 is based on an overall database of 898 tests including mass losses up to about 82% so it is deemed to have a reasonably wide domain of applicability. Moreover, it offers a modeling flexibility consistent with the limited information that one could expect from in-situ surveys. In fact, an inspector would likely characterize the corrosion of an element by assessing diameter loss in a few bars from the more corroded regions and, sometimes, integrating this with a few punctual measures of concrete carbonation or chlorides concentrations. Based on this type of information, the inspector can, through its expert judgment, qualify the corrosion level by first discriminating between uniform and pitting corrosion and, in case of occurrence of the latter, between mild, average or strong pitting.

Figure 7 plots the yield stress and ultimate strain reduction coefficients of the new laws as a function of ψ. This shows that, although mild pitting is essentially equivalent to uniform corrosion, average and strong pitting yield significantly bigger degradations that quickly increase with mass loss.

4.1.2 | Degradation laws for unconfined concrete

Cover concrete deterioration is due to the volumetric expansion of corrosion products that generates transversal principal tensile strains ε_1 and generating the, so-called, softening effect. Coronelli and Gambarova[20] proposed to use the results of smeared stress–strain models to describe this softening. The key point in the use of such models is to express ε_1 as a function of the crack width w_{cr} which, when multiplied by the number of bars n_b and divided by the corresponding bar spacing i_b, can be interpreted as the smeared tensile strain acting orthogonally to compression:

$$\varepsilon_1 = \frac{n_b w_{cr}}{b} = \frac{w_{cr}}{i_b} \tag{7}$$

Several theories have been proposed to correlate w_{cr} with ψ(see e.g., reference [21]), however the various models can give rather different predictions depending on the situations.[22] Moreover the w_{cr}–ψ correlations generally depend on the bar diameter, a fact that would significantly complicate the material parameters management. For such reasons, we propose to use directly w_{cr} as DIM for UC regions. This choice is well suited in the present context also because approximate values of w_{cr} could be estimated in-situ through visual inspection. To this end, it is important to stress that visual inspection must unavoidably be complemented with hammering of concrete surfaces or other techniques useful to detect the eventual presence of delaminations that could hide cover cracking to the inspector.

The parameter most influenced by degradation is compressive peak stress f_{cp} and to a lesser extent peak strain ε_{su}, for wich degradation laws can be put in the form:

$$f_{cp,D} = \left(K_{f_{cp}}\right) f_{cp,P},\ \varepsilon_{cp,D} = \left(K_{\varepsilon_{cp}}\right) \varepsilon_{cp,P} \tag{8}$$

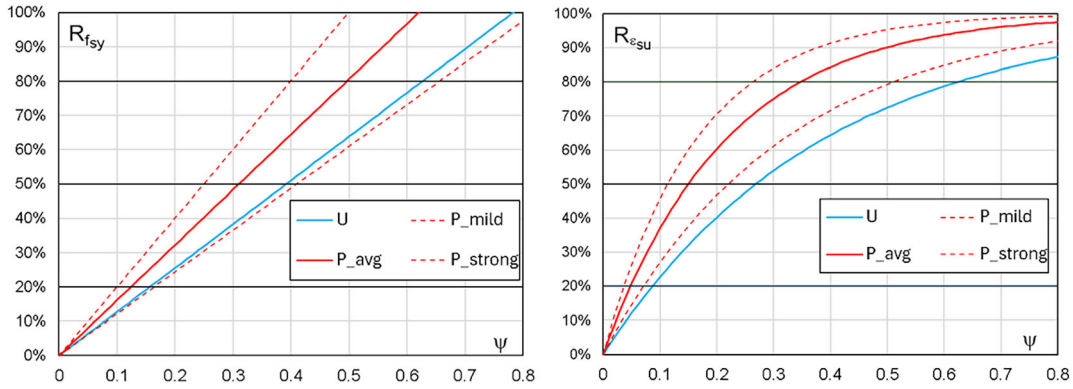

FIGURE 7 Proposed degradation laws in terms of reduction factors $R_{f_{sy}} = 1 - K_{f_{sy}}$ and $R_{\varepsilon_{su}} = 1 - K_{\varepsilon_{su}}$.

TABLE 5 Selected degradation laws for UC.

	$K_{f_{cp}}$	$K_{\varepsilon_{cp}}$
Vecchio-Collins (Model B) (VC)	$\frac{1}{1+0.27\left(\frac{w_{cr}}{i_b \varepsilon_{cp,P}}-0.37\right)}$	1
Belarbi-Hsu (VG)	$\frac{0.9}{\sqrt{1+400\frac{w_{cr}}{i_b}}}$	$\frac{1}{\sqrt{1+550\frac{w_{cr}}{i_b}}}$
Coronelli-Gambarova (CG)	$\frac{1}{1+C\left(\frac{w_{cr}}{i_b \varepsilon_{cp,P}}\right)}$	$K_{f_{cp}}$

Various laws have been proposed and Table 5 summarizes three of them.

All models depend on bar spacing and Figure 8 plots strength reduction factor against w_{cr} for different spacings. CG model is plotted both with the, often used, value $C = 0.1$ as well $C = 0.2$. The comparison shows that the first value tends to underestimate degradation with respect to the other ones, whereas $C = 0.2$ seems to be in better agreement with the other models and, for this reason, this value is considered in the following.

4.1.3 | Deterioration of confined concrete

Confinement is the result of purely mechanical interactions between stress and strain components acting along orthogonal directions. In a FB setting this is modeled indirectly by a *confinement model* providing an estimate of the lateral pressure exerted by transversal reinforcement and of the properties of the confined concrete as a function of those of transversal steel, unconfined concrete and reinforcement layout.

The physical process underlying confinement is not directly influenced by corrosion which, on the other hand, has a direct effect on transverse reinforcement and unconfined concrete. Therefore, deteriorated confined concrete can be modeled by standard confinement models, provided material parameters are obtained via degradation laws for core concrete and stirrups.

The local deterioration level of a CC region is thus determined by two DIM: w_{cr} defining deterioration of the underlying unconfined concrete and mass loss ψ_T of the transversal reinforcement determining stirrups corrosion. As discussed in Section 4.5, the determination of the two DIM is different because w_{cr} depends directly on the exposition zone of the CC region, whereas ψ_T depends on the exposition zones of the exposed legs of the stirrups present in the UCZ to which the region belongs.

4.2 | Local deterioration scale for regions

Although in laboratory tests, DIM can be measured with precision, in actual engineering applications they have to be estimated from limited information collected in-situ. Therefore, instead of precise DIM values, it is likely that the local deterioration level of the materials would be encoded by a qualitative expert judgment formulated by an inspector based on the overall consideration of the deterioration state.

To incorporate this aspect in the modeling framework, it is useful to define a *local deterioration scale* articulated in levels of increasing deterioration. While the qualitative definition of the scale is trivial, the crucial point is how to convert it into a quantitative one. To solve this problem, we propose to invert the chosen degradation laws to determine the range of DIM which corresponds to a given range of reduction of the material property. Scales articulated in 8 levels are proposed in the left parts of Tables 6 and 7 where, for example, a medium deterioration corresponds to a reduction of the material properties in the range 20%–50% (further articulated in three sublevels) and so on for the other levels. Clearly, scales with different numbers of levels can be proposed.

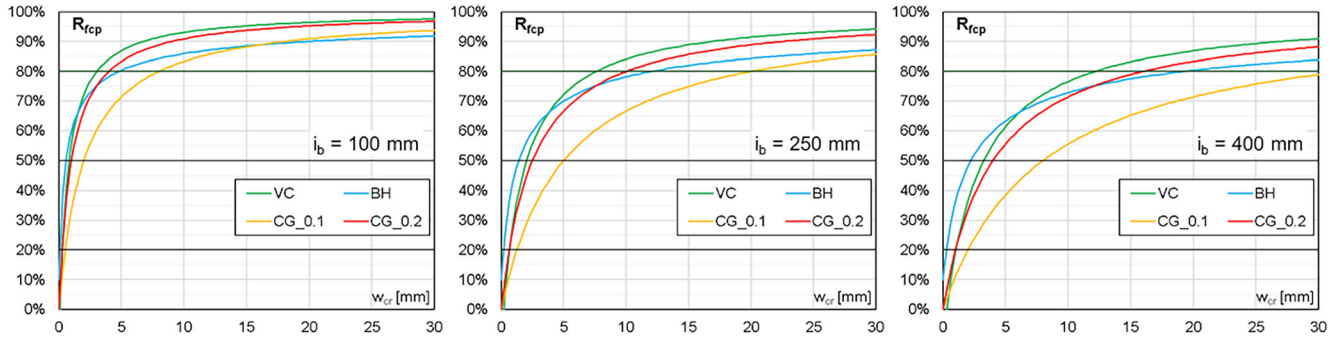

FIGURE 8 Degradation laws for UC for different bar spacing $i_b, \varepsilon_{cp} = 0.002$ in terms of $R_{f_{cp}} = 1 - K_{f_{cp}}$.

TABLE 6 Local deterioration scale for LS regions based on percentual reductions of f_{sy} and f_{su} according to the steel degradation laws proposed in Section 4.1.1.

			Quantitative LDI for LS regions [mass loss ψ]			
				Pitting corrosion		
Qualitative LDI		Material property reduction (f_{sy},f_{su})	Uniform corrosion	Mild	Average	Strong
Low		<20%	<0.15	<0.15	<0.12	<0.10
Medium	a	20–30%	0.15–0.25	0.15–0.25	0.12–0.20	0.10–0.15
	b	30–40%	0.25–0.30	0.25–0.30	0.20–0.25	0.15–0.20
	c	40–50%	0.30–0.40	0.30–0.40	0.25–0.30	0.20–0.25
High	a	50–60%	0.4–0.50	0.40–0.50	0.30–0.35	0.25–0.30
	b	60–70%	0.50–0.55	0.50–0.60	0.35–0.40	0.30–0.35
	c	70–80%	0.55–0.65	0.60–0.65	0.40–0,50	0.35–0.40
Extreme		>80%	>0.65	>0.65	>0.5	>0.40

Note: Low level should be yellow, Medium: orange, High: red, Extreme; black. Darker background colors should have text with white font.

TABLE 7 Local deterioration scale for UC regions based on percentual reductions of f_{cp} according to Coronelli-Gambarova law with $C = 0.2$ and $\varepsilon_{cp} = 0.002$.

			Quantitative LDI for UC regions [w_{cr} in mm]						
			Bar spacing [cm]						
Qualitative LDI		Material property reduction (f_{cp})	10	15	20	25	30	35	40
Low		<20%	<0.3	<0.4	<0.5	<0.6	<0.8	<0.9	<1.0
Medium	a	20–30%	0.3–0.4	0.4–0.6	0.5–0.9	0.6–1.1	0.8–1.3	0.9–1.5	1.0–1.7
	b	30–40%	0.4–0.7	0.6–1.0	0.9–1.3	1.1–1.7	1.3–2.0	1.5–2.3	1.7–2.7
	c	40–50%	0.7–1.0	1.0–1.5	1.3–2.0	1.7–2.5	2.0–3.0	2.3–3.5	2.7–4.0
High	a	50–60%	1.0–1.5	1.5–2.3	2.0–3.0	2.5–3.8	3.0–4.5	3.5–5,3	4.0–6.0
	b	60–70%	1.5–2.3	2.3–3.5	3.0–4.7	3.8–5.8	4.5–7.0	5.3–8.2	6.0–9.3
	c	70–80%	2.3–4.0	3.5–6.0	4.7–8.0	5.8–10.0	7.0–12.0	8.2–14.0	9.3–16.0
Extreme		>80%	>4.0	>6.0	>8.0	>10.0	>12.0	>14.0	>16.0

Note: Low level should be yellow, Medium: orange, High: red, Extreme; black. Darker background colors should have text with white font.

Once a qualitative level is associated to a range of reduction of the material property, then the degradation law determines a specific range of DIM, called *Local Deterioration Index* (LDI).

The quantitative scale for steel regions based on the degradation laws proposed in Section 4.1.1 is described in the right part of Table 6 and can be graphically visualized in Figure 7 through the intersections of the bold

horizontal lines with the corresponding reduction curves. The mass loss ranges are computed by inverting the degradation laws for yield and ultimate stress, taking the mean value (of the mass losses corresponding to the reductions of f_{sy} and f_{su}) and approximating the results to multiples of 0.05. Assigning mass losses in this way, the actual reduction in yield stress and strength can be directly controlled. Of course, the corresponding reduction in ultimate strain is determined by the corresponding law.

The table shows, for example, that a medium local deterioration level for LS regions (defined as the one that produces a reduction of yield and peak stress within 20%–50%) is produced by different mass losses, depending on the type of corrosion. In particular, in presence of uniform corrosion this level of deterioration is produced by mass losses between 0.15 and 0.40. On the other hand, in presence of strong pitting the same deterioration level is reached for much smaller mass losses (0.10–0.25). In other words, the same corrosion intensity, can produce different local deterioration levels depending on the type of corrosion. For example, a mass loss of 0.4 associated with strong pitting produces extreme deterioration, while it produces medium deterioration if corrosion is uniform.

A similar discussion can be done for UC regions. The quantitative scale for unconfined concrete regions based on the degradation laws proposed in Section 4.1.2 (i.e., Coronelli-Gambarova model with $C = 0.2$) is described in the right part of Table 7 and can be graphically visualized in Figure 8 through the intersections of the bold horizontal lines with the corresponding reduction curves. Each LDI now corresponds to a range of w_{cr} computed by inverting the degradation law for any given value of bar spacing and concrete peak strain.

The table shows, for example, that a medium local deterioration level for UC regions (defined as the one that produces a reduction of compressive strength within 20%–50%) is produced by different w_{cr}, depending on bar spacing. In particular, for a spacing of 10 cm this level of deterioration is produced by w_{cr}, between 0.3 and 1.0 mm, according to the chosen degradation law. On the other hand, in presence of a large bar spacing of 50 cm the same deterioration level is reached for much bigger w_{cr} (1.3–5.0 mm). In other words, the same w_{cr}, can produce different local deterioration levels depending on the bar spacing. For example, a w_{cr} of 1 mm with a bar spacing of 10 cm produces high deterioration, whereas it produces a low deterioration for larger spacing.

The values reported in the table have to be interpreted as equivalent values to be specified in order to obtain, with the given degradation laws, a prescribed level of deterioration over a potentially large zone of unconfined concrete. It is expected that the high values associated to larger spacings will be used seldom in practice because it is unlikely that severe cover concrete deterioration would occur when the bars are far from each other.

4.3 | Global deterioration scale for zones

The scales defined in the previous section provide a way to correlate qualitative judgments on the deterioration of the materials with quantitative ranges of the damage intensity measures (i.e., ψ or w_{cr}) in a way consistent with the chosen degradation laws. However, in the development of the models for real structures it is rarely the case that this type of judgment can be given locally on each region. On the contrary, in practical situations, it is likely that an inspector would evaluate the global deterioration level of an exposition zone composed of regions characterized by a similar influx of corrosive agents. In this case, the local deterioration level of the regions belonging to the zone cannot be specified arbitrarily but should reflect a consistent state of damage.

To this end, it is useful to define a *global deterioration scale* articulated in stages of increasing deterioration for the zones and characterized by macroscopic features that could be detected in-situ. Hereafter a possible sequence of stages is proposed, although several alternatives are possible:

- Stage 1: Volumetric expansion of corrosion products produces micro and macro cracking in concrete cover (Figure 9). At this stage, unconfined concrete presents a low/medium level of deterioration corrosion which

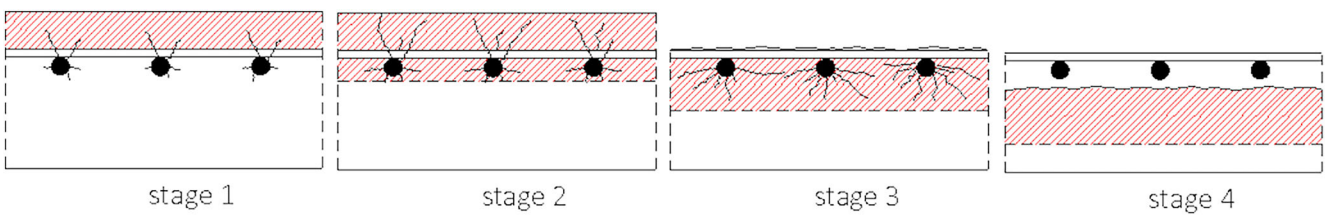

FIGURE 9 Schematic illustration of stages of the deterioration progression.

could be associated with low and low/medium deterioration of longitudinal bars and stirrups, respectively. According to Table 7, this type of deterioration of UC can be determined by small cracks if bars are tightly spaces or by larger cracks if bar spacing is higher. Therefore, an inspector, knowing bar spacing, can evaluate the occurrence of this stage by visual or instrumental evaluation of cover concrete cracking. This can be complicated in presence of delamination when cracks may be present but invisible from outside. In this case, additional tests like simple superficial hammering or GPR scans could be used to assess the eventual presence of delamination.[23] However, since Stage 1 corresponds to the lowest level of deterioration progression, which presumably produces a limited impact on the capacity of the structure, the recourse to more expensive diagnostics could be not worth the benefit. In this case, Stage 1 can be ascertained by the absence of signs of more severe stages.

- Stage 2: Corrosion of rebars increases, concrete cover is severely cracked or delaminated, a thin layer of confined core may also be slightly cracked (Figure 9). At this stage, UC presents a medium/high level of deterioration which could be associated with medium and medium/high deterioration of longitudinal bars and stirrups, respectively. In absence of delamination this can be visually detected by stirrups that are barely visible or partially exposed. In presence of delamination, this stage can be detected by hammering.
- Stage 3: Bars are highly corroded, cover is spalled or delaminated, the depth of deteriorated layer of the confined core increases[24] (Figure 9). At this stage, cover is spalled or can be removed after hammering, stirrups are completely exposed and longitudinal bars can be visible or partially exposed.
- Stage 4: The boundary of confined core becomes directly exposed to environmental actions (Figure 9). At this extreme stage, both longitudinal bars and stirrups give a negligible contribution to the sectional capacity and confined core reduces its size.

Each stage of the progression can be associated with a *Global Deterioration Index* (GDI) which consists in the assignment of a qualitative LDI for each material of the zone. Table 8 shows a possible definition for a global scale where stages 1, 2, 3 are further partitioned in sublevels. Of course, differently motivated definitions of deterioration progression are possible and scales different from Table 8 can emerge.

Once a GDI has been assigned to an exposition zone then, using the local deterioration scales (Tables 6 and 7), a specific value of the damage intensity measure (ψ, w_{cr}) can be assigned to each region of LS and UC in the zone,

TABLE 8 Illustrative example of a possible global deterioration scale consistent with the above definition of the deterioration progression.

		LDI for region materials		
GDI	**Stage**	**LS**	**TS**	**UC**
0	0	Plain	Plain	Plain
1	1.a	Low	Low	Low
2	1.b	Low	Medium	Medium
3	2.a	Medium	Medium	Medium
4	2.b	Medium	High	High
5	3.a	High	High	Extreme
6	3.b	High	Extreme	Extreme
7	4	Extreme	Extreme	Extreme

Note: Columns indexed by 0: green, 1 and 2: yellow, 3 and 4 orange, 5: red, 6: purple, 7: lack. Darker background colors should have text with white font.

by taking a representative value within the interval, as, for example, the average one. The assignment of DIM to CC region is described in Section 4.5.

The crucial point in the definition of the global deterioration scale is the association between the LDI of cover concrete with the one of longitudinal and transversal steel. Of course, this is a very complex problem and a precise solution could be obtained only in special cases on the basis of detailed analyses. The proposed simplified definition, summarized in Table 8, follows from plausible hypotheses potentially verifiable using the limited information available in practical cases. If, in the future, more advanced diagnostics would be amenable to routinary use, more detailed and precise definitions of local and global deterioration scales will be possible. Detailed numerical simulations of diffusion of aggressive agents could also help to define more specific scales.

4.4 | Deterioration attenuation law

The direct assignment of a GDI is possible, to within the limits and the approximations outlined above, only for the zones in the exposed layer. However, to model a corroded RC structure, deterioration has to be specified also in the interior of the structure. As discussed in Section 2.2, exposition zones are stratified in a sequence of layers partitioned into aggression paths, where levels of the same depth can be assumed, for the purpose of modeling, to be subject to similar influx of aggressive agents.

Deterioration penetration beyond external surface can then be modeled by a *deterioration attenuation law* consisting of a sequence of GDI for each level of the stratification. Clearly, the definition of such a law is a very

TABLE 9 Illustrative example of a possible deterioration attenuation law.

	Exposed layer	Superficial layers					Internal zone
Layer depth	**0**	**1**	**2**	**3**	**4**	**5**	**-**
	0	0	0	0	0	0	0
	1	0	0	0	0	0	0
	2	0	0	0	0	0	0
	3	2	0	0	0	0	0
	4	3	2	0	0	0	0
	5	4	3	2	0	0	0
	6	5	4	3	2	0	0
	7	6	5	4	3	2	0

Note: Columns indexed by 0: green, 1 and 2: yellow, 3 and 4 orange, 5: red, 6: purple, 7: lack. Darker background colors should have text with white font.

complex problem and a precise solution could be obtained only in special cases on the basis of detailed information by means of specific diffusivity analyses (e.g., Fick's law). In absence of more precise information, a sequence of progressively less severe GDI with the increase of depth can be hypothesized heuristically based on the consideration of factors like aggressivity of the external environment, concrete porosity and permeability. It is hoped that future research could lead to more specific definitions based on numerical simulations (e.g., 3D multi-physics models) supported by advanced in situ-experimental measurements.

To illustrate the idea, Table 9 shows a possible heuristic attenuation law applicable to a stratification in five superficial layers. Values in the rows of the table are the GDI of the various layers. Clearly, the definition of the thickness of each layer is a modeling choice depending on the specific structural and environmental conditions. Other laws appropriate for stratifications with a lower number of layers can be defined in a similar way.

4.5 | Determination of DIM from GDI

Once a deterioration attenuation law is defined, the GDI of all zones can be determined, to within the limits and the approximations outlined above, from the knowledge of those of the exposed layers and this is sufficient to assign specific values of DIM to every region according to the following procedure.

For UC and LS regions the values of w_{cr} and ψ_L are derived directly from the GDI assigned to their exposition zone, according to the depth of their level.

For CC regions, the situation is different since two DIM need to be specified. The value of w_{cr} can be determined directly from the GDI of its exposition zone. On the contrary, due to confinement non-locality, ψ_T depends on the corrosion of all legs of the stirrup which may be located in different exposition zones. As discussed in Section 2.1 every CC region belongs to a Uniform Confinement Zone and every UCZ is assumed to have a common peripheral stirrup. The value of ψ_T can then be determined from the most severe GDI among those assigned to the all exposition zones traversed by the stirrup.

TABLE 10 Nomenclature for parameters (entries of the lists depend on the specific material and confinement model).

Region	Plain	Deteriorated
LS	**par_LP**	**par_LD**(ψ_L)
UC	**par_UP**	**par_UD**($w_{cr,U}$)
CC	**par_TP** + **par_UP** + **par_G**	**par_TD**(ψ_T) + **par_UD** ($w_{cr,C}$) + **par_G**

5 | MATERIAL PARAMETERS MANAGEMENT

The proposed modeling approach can be implemented as an algorithm to manage material parameters of regions. Regions parameters are denoted **par_L**, **par_U**, **par_C**, respectively for LS, UC and CC regions. Parameters for CC regions are derived from a confinement model taking as input parameters **par_T** of transversal reinforcement and **par_G** of stirrups layout (e.g., diameter and spacing of stirrups, number of legs, spacing between constrained longitudinal bars). Taking into account deterioration, 6 groups of parameters needs to be specified (Table 10).

The flow-chart in Figure 10 summarizes the algorithm underlying the proposed modeling approach. Given the GDI of the exposed layers and the exposition parameters of the regions, the attenuation law

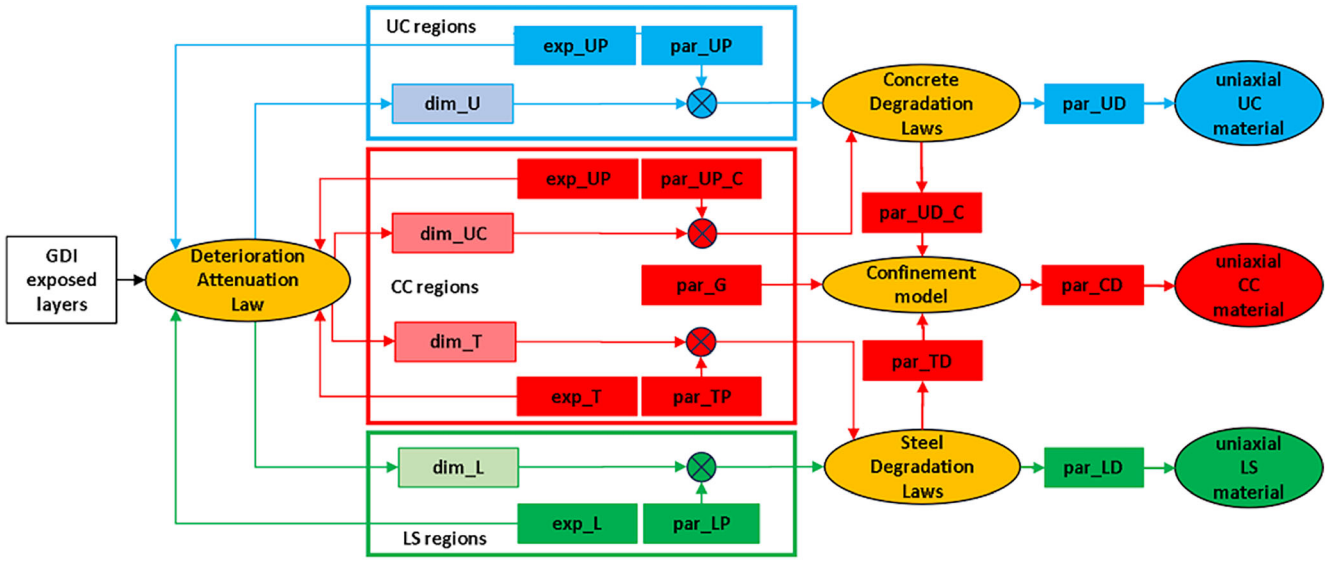

FIGURE 10 Conceptual scheme of the algorithm for material parameters management.

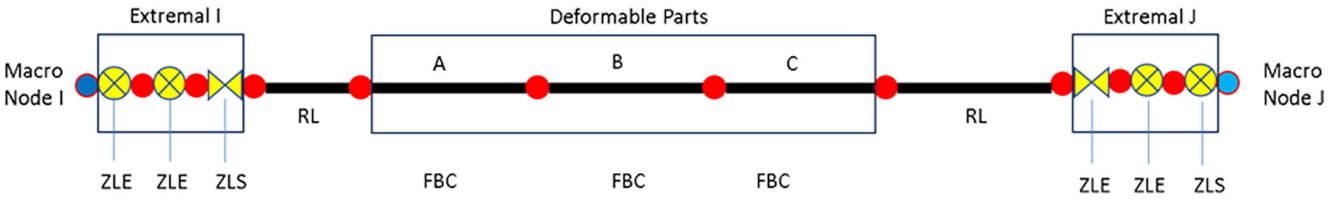

FIGURE 11 Conceptual scheme of the OpenseesPy macro-element of a non-uniformly corroded beam column composed by three deformable parts.

determines the DIM of the regions. Degradation laws, taking as input DIM and uncorroded parameters, provides the parameters for the deteriorated regions that can be finally passed to the uniaxial stress–strain laws.

6 | AN OpenseesPy MACROELEMENT OF CORRODED BEAM-COLUMN

The proposed approach has been implemented in OpenseesPy as a macroelement of arbitrarily corroded beam-column (Figure 11). The macroelement is a flexible modeling tool that can be used in a variety of situations. It is characterized by two macro-nodes connected by several elements customizable to model different scenarios. Macroelements can be used alone to model, for example, a single-column pier or arranged in various ways to model multiple-columns piers or framed structures.

A macro element represents a piece, in the terminology of Section 3, and can be composed by one or more force-based beam-column (FBC) elements each one characterized by a different fiber section. The number of deformable parts depends on the complexity of the elevation deterioration pattern. In many cases, three parts suffice, but more complex patterns may require more of them. To complete the modeling, each macroelement includes two extremely zones each one composed of up to three zero length (ZL) elements and a rigid link. The ZL elements can be used, if necessary, to model bond-slip phenomena, shear deformability or geotechnical stiffnesses (Section 6.1). Rigid links, may be needed in some cases to model pier caps or eccentricities within elements of a framed structure (Figure 11).

The input of corroded sections is encoded in a spreadsheet file which describes regions connectivity (concrete geometry and reinforcement layout), sectional deterioration patterns, uniform confinement zones and the stratification in exposition layers. So far, four types of sections have been implemented: solid and hollow rectangular, solid and hollow circular. The macroelement has been coded in several Python classes interacting with a command wrapper called Meta-OpenSees. The classes have customizable attributes that allow the user to choose

among several options concerning uniaxial stress–strain laws, confinement models, integration algorithms, bond-slip models (Section 6.1), density of concrete fiber discretization as well as other modeling options.

The classes have been included within a larger Python application (named CP for 'Corroded Piers') capable to carry out pushover analyses of corroded structures. In this app, several macroelements can be combined, loads and restraints can be applied to macronodes, running analyses with monotonic or cyclic displacement histories.

During the solution, a step-by-step control of axial strains in all fibers of the model is carried out. Fibers strains are then used to monitor the occurrence of an arbitrary number of events related to RC behaviors (e.g., cracking, yielding, bending or shear failure, prescribed strain levels of steel and concrete).

Special attention has been paid to the issues related to numerical curvature localization in presence of material softening. The integration schemes proposed in references [25,26] have been implemented in the macroelement. Both of them achieve objectivity of solution (i.e., independence of the results on the number of integration points) and can be used according to convenience. Both schemes depend on two algorithmic parameters: one correlated with the plastic hinge length and the other defining the position of the additional integration points. Accuracy of numerical solution can be evaluated a posteriori by inspection of curvature profiles along the elements.

6.1 | Modeling of additional phenomena

Standard FB finite elements take into account axial and flexural response. However, the highly nonlinear behavior of RC is characterized by additional phenomena that can be taken into account in various ways.

Bar buckling can be implemented by modifying steel stress–strain law in compression as a function of bar slenderness ratio[27] and by adding low-cycle fatigue elements. Various modeling options have been evaluated but their implementation within the macroelement is still ongoing.

Shear deformability can be modeled by means of nonlinear springs calibrated on empirical estimates of the stiffness before and after shear cracking.[28] This effect will be implemented in the macroelement in one of the ZL elements activable at the ends.

Strain penetration effects associated with bond-slip can be modeled by modifying steel stress–strain laws[29] or by adding ZL elements with overall moment–rotation response evaluated by macromodels like reference [30]. Alternatively, the link behavior can be obtained from a fiber section with the same geometry of the adjacent section provided the steel regions are characterized by a stress-slip relation again derived from macro-models like reference [30] or [31]. In this case, to accommodate large compressive strains induced by steel slips, concrete fibers in the ZL are modeled by an uniaxial law with limited softening, zero tensile strength and ultimate strains scaled proportionally to the ratio between slip displacement at yield and steel yield strain, as suggested by LeBorgne and Ghannoum.[32] Other macro-models capable to take into account the influence of corrosion on bond (e.g. reference [33]) will be implemented in future versions to obtain more refined stress-slip relationships.

Shear failure can be modeled by comparison between the bending response and a model for shear capacity. In the macroelement, shear capacity is computed step-by-step and used to look for intersections with flexural response to detect eventual shear failure. Capacity models[34,35] are used for hollow rectangular and circular sections respectively, whereas reference [36] is used for other sections.

7 | EXPERIMENTAL VALIDATION

To validate the proposed approach, 16 experimental tests of RC elements subject to lateral loads have been selected to include different sections (solid and hollow rectangular, solid circular), reinforcement ratios (0.9%–1.6%), axial load ratios (5%–40%), as well as different confinement levels (Table 11, Figure A1). Experimental tests include several corroded structures with average mass loss up to 25% as well as uncorroded cases useful for the sake of comparison.

The information available in the referenced papers about corrosion intensity and degradation has been used to estimate the GDI of the external surfaces (Table 12).

For tests taken from Guo et al.,[37] information from figures 2–6 as well as table 1 in reference [37] was used to assess global deterioration level. Based on this, evidence of strong pitting and higher corrosion of stirrups with respect to bars was deduced. From the information about mass losses in table 1 of reference [37] that, in situ could be estimated by random sampling of residual bar diameters, specimens S2, S3, S4 were considered to be consistent with stages 1.b, 2.a and 2.b, corresponding to GDIs 2, 3, 4, more specifically articulated as in Table 12.

For tests taken from Rinaldi et al.[38] information from figures 3, 4, 12 and table 1 in reference [38] was used to assess global deterioration level. Based on this, evidence

TABLE 11 Main features of the specimens.

Source	Specimen ID	Section	H (m)	Size (mm)	f_{cp_UP} (MPa)	Longitudinal reinforcement			Transversal reinforcement		ALR (%)
						ρ_L (%)	f_{sy_LP} (MPa)	f_{su_LP} (MPa)	Stirrups (mm)	f_{sy_TP} (MPa)	
Guo et al.[37]	S1	SR	2.3	650 × 250	42.9	1.6	362	505	Φ8/60–100	325	10
	S2	SR	2.3	650 × 250	42.9	1.6	362	505	Φ8/60–100	325	10
	S3	SR	2.3	650 × 250	42.9	1.6	362	505	Φ8/60–100	325	10
	S4	SR	2.3	650 × 250	42.9	1.6	362	505	Φ8/60–100	325	10
Rinaldi et al.[38]	A25	SS	1.5	300 × 300	25	0.9	520	600	Φ8/250	520	16
	B25	SS	1.5	300 × 300	25	0.9	520	600	Φ8/250	520	16
	A30	SS	1.5	300 × 300	25	0.9	520	600	Φ8/300	520	16
	B30	SS	1.5	300 × 300	25	0.9	520	600	Φ8/300	520	16
Ma et al.[39]	C0-15	SC	1.0	260	32.4	1.1	373.2	572.3	Φ8/100	327	15
	C9-15	SC	1.0	260	32.4	1.1	373.2	572.3	Φ8/100	327	15
	C0-25	SC	1.0	260	32.4	1.1	373.2	572.3	Φ8/100	327	25
	C9-25	SC	1.0	260	32.4	1.1	373.2	572.3	Φ8/100	327	25
	C0-40	SC	1.0	260	32.4	1.1	373.2	572.3	Φ8/100	327	40
	C9-40	SC	1.0	260	32.4	1.1	373.2	572.3	Φ8/100	327	40
Lignola et al.[40]	NC	HR	1.5	600 × 400	17	0.9	505	620	Φ3/120	655	5
	C	HR	1.5	600 × 400	20.7	0.9	505	620	Φ3/120	655	5

Abbreviations: HR, hollow rectangular; SC, solid circular; SS, solid square.

TABLE 12 GDIs and corresponding values of DIMs for the tested specimens.

Authors	Specimen ID	Stage	GDI	Corrosion type		LS	TS	UC	i_b (cm)	ψ_L (%)	ψ_T (%)	w_{cr} (mm)
Guo et al.[37]	S1		0	-	-	-	-	-	10	0	0	0
	S2	1.b	2	Pitting	Strong	Low	Med.a	Med.a	10	5	12.5	0.35
	S3	2.a	3	Pitting	Strong	Med.a	Med.b	Med.b	10	12.5	17.5	0.55
	S4	2.b	4	Pitting	Strong	Med.b	High.a	High.a	10	17.5	27.5	1.25
Rinaldi et al.[38]	A25	-	0	-	-	-	-	-	20	0	0	0
	B25	2.a	3	Pitting	Strong	Med.c	Med.c	Med.a	20	22.5	22.5	0.7
	A30	-	0	-	-	-	-	-	20	0	0	0
	B30	2.a	3	Pitting	Strong	Med.c	Med.c	Med.a	20	22.5	22.5	0.7
Ma et al.[39]	C0-15	-	0	-	-	-	-		15	0	0	0
	C9-15	2.a	3	Pitting	Strong	Med.a	Med.b	Med.b	15	12.5	17.5	0.8
	C0-25	-	0	-	-	-	-		15	0	0	0
	C9-25	2.a	3	Pitting	Strong	Med.a	Med.b	Med.b	15	12.5	17.5	0.8
	C0-40	-	0	-	-	-	-		15	0	0	0
	C9-40	2.a	3	Pitting	Strong	Med.a	Med.b	Med.b	15	12.5	17.5	0.8
Lignola et al.[40]	NC	-	0	-	-	-	-	-	10	0	0	0
	C	2.a	3	Pitting	Average	Med.a	Med.b	Med.b	10	16	22.5	0.55

of strong pitting and no evidence of higher corrosion of stirrups with respect to bars were deduced. From the information in table 2 of reference [38], specimens B25 and B30 were considered to be consistent with stage 2.a, corresponding to GDI 3, more specifically articulated as in Table 12.

For tests taken from Ma et al.[39] information from figure 4 and table 1 in the paper [39] was used to assess global deterioration level. Based on this, evidence of strong pitting and higher corrosion of stirrups with respect to bars was deduced. From the information in table 2 of reference [38], specimens C9-15, C9-25 and C9-40 were considered to be consistent with stage 2.a corresponding to a GDI 3, more specifically articulated as in Table 12.

For tests taken from Lignola et al.[40] information from textual descriptions in sections 6 and 7 of reference [40] was used to assess global deterioration level. In absence of more specific information, an average pitting corrosion was assumed. Higher corrosion of stirrups with respect to bars was indirectly deduced from the text. Specimen C was then considered to be consistent with stage 2.a corresponding to a GDI 3, more specifically articulated as in Table 12.

It is very important to note that, in all cases, damage intensity measures (i.e., mass losses and w_{cr}) were determined according to the corresponding local deterioration scales. Specifically, Table 6 for steel and Table 7 for unconfined concrete. The obtained values are sometimes different from the measured average values and are reported in Table 12.

The accuracy of the numerical predictions is evaluated with respect to peak force and ultimate drift. The latter evaluated at the first occurrence of either failure or 85% of strength. Since a significant loading direction asymmetry is observed in most cases, the comparison refers to the direction giving best accuracy on strength.

It is important to remark that the validation is not aimed to reach the best possible accuracy, that could be obtained, for example, by specifying the measured mass loss for each bar. The goal of the validation is to check the accuracy that can be obtained by using the approximated deterioration scales defined above, neglecting mass loss variability over the bars. To this end, models were developed, by identifying the GDI as discussed above with the rest of the parameters determined according to the deterioration scales and attenuation laws proposed in previous sections.

An overall summary of the results in terms of strength and ultimate drift is reported in Table 16. In the next Sections the attention is focused on the ability of the modeling to properly take into account the influence of the following main aspects: corrosion intensity, axial load, non-uniformity of sectional corrosion, confinement level.

7.1 | Specific modeling assumptions

For this validation, a model composed of a single macroelement with two deformable parts is used for all cases, as this enough to describe the patterns considered in the experimental tests.

Fibers of UC, CC, LS regions are modeled by OpenSees uniaxial materials *Concrete02*, *Concrete04*, *Steel02*. While other material models can be selected in the macroelement, the above choices are presented because this validation aims to assess the accuracy of the

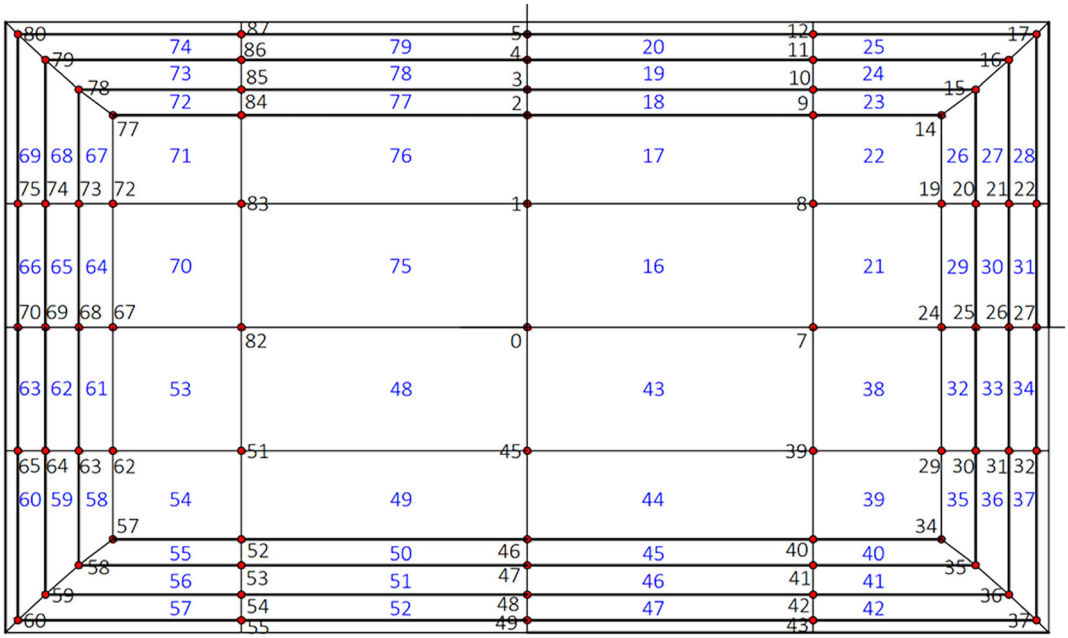

FIGURE 12 Scheme of the partition of the solid rectangular sections into CC regions (not to scale).

modeling approach using standard material assumptions. For CC regions, parameter r is calibrated as $E_{c,sec}/E_c$ with degradated concrete parameters and using Mander confinement model. Cyclic parameters have been set up to the default values specified in the OpenSees documentation without further refinement since the validation is not focused on the details of the cyclic response.

Degradation laws for steel are the new relations proposed in Section 4.1.1, used by choosing the type of corrosion on the basis of the information that can be deduced from the papers. Degradation law for unconfined concrete is Coronelli-Gambarova used according to Section 4.1.2 and the actual bar spacing.

Solid rectangular (circular) sections are partitioned in 20 (10) UC regions and 60 (30) CC regions (Figures 12 and 13). Steel regions have been discretized by using a fiber per each bar. Concrete regions are internally discretized by using quadrilateral or circular patches with average size of about 20 mm. Confined concrete regions are grouped in a single UCZ.

Exposition zones are partitioned in a stratification composed of three superficial levels. The attenuation law decreases the GDI by one level for each depth level in the stratification.

Bond-slip is modeled by activating a ZL element at the base, whose steel bars have a *Hysteretic* material calibrated with the stress-slip law derived by the standard Sezen-Setzler model. Concrete fibers in the ZLS are modeled by *Concrete02* adopting the precautions discussed in Section 6.1.

No rigid links, nor other ZL elements are activated in the macroelement.

Bending failure is determined by the attainment of ultimate strains in LS or CC regions according to the event which occurs first. Ultimate tensile strain for steel

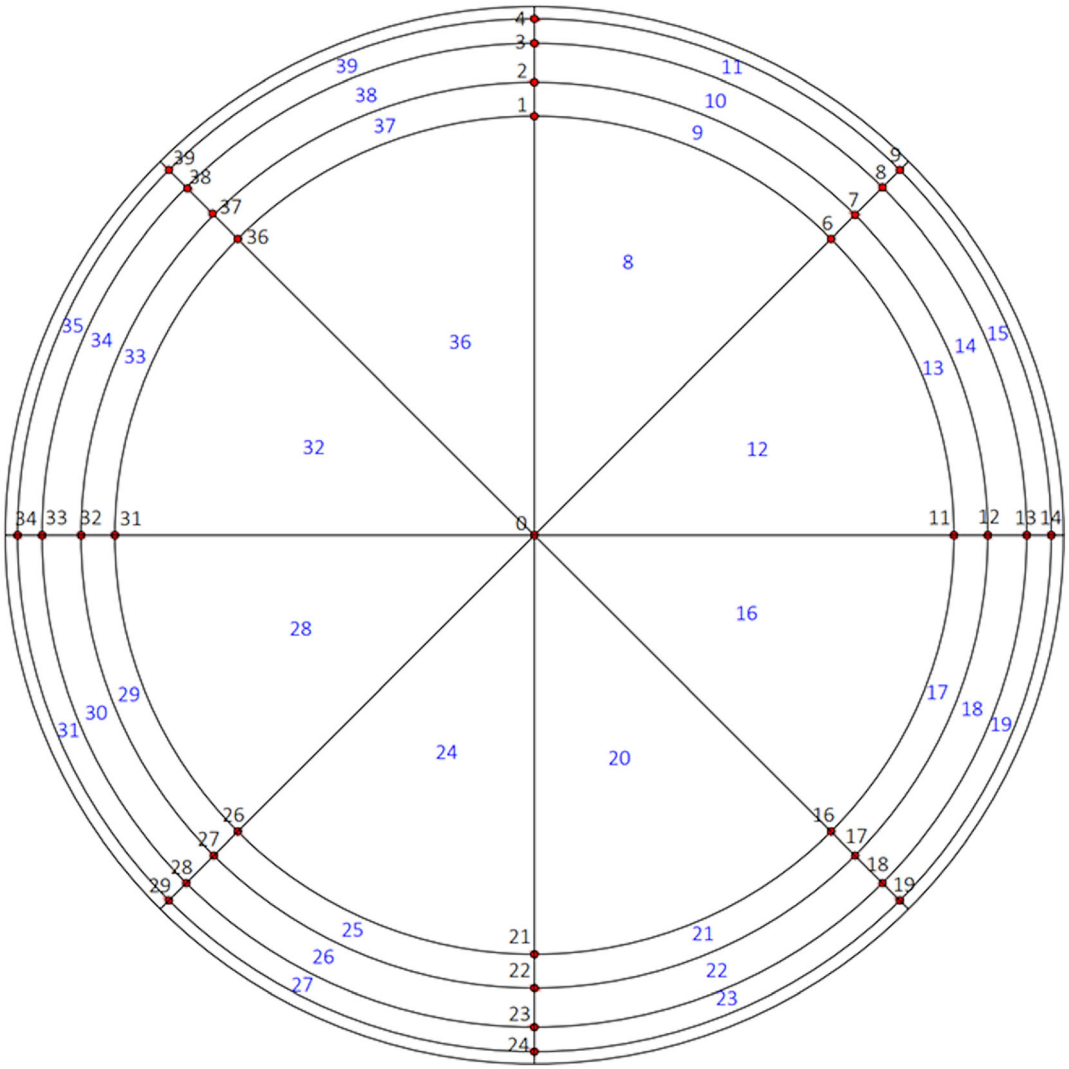

FIGURE 13 Scheme of the partition of the solid circular sections into CC regions (not to scale).

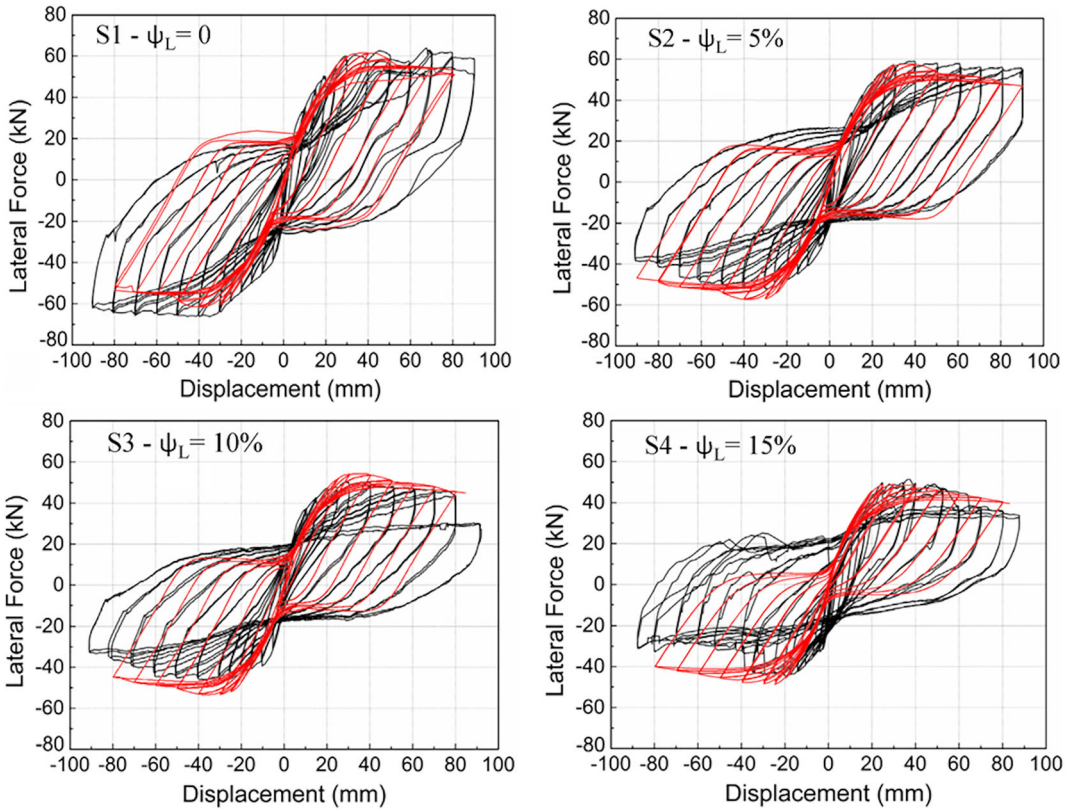

FIGURE 14 Tests S1–S4 from Guo et al.[37] Mass losses shown in the plots are those corresponding to expected values considered in the design of artificial corrosion process.

is $\varepsilon_{su} = 0.12$ for uncorroded bars, whereas reduced values evaluated according to the degradation laws proposed in Section 4.1.1 are used for corroded bars. Ultimate compressive strain for confined concrete is determined by Priestley formula with parameters for steel and concrete degradated according to the procedure described in Section 4.1.3. Shear failure is evaluated by intersecting the flexural curve with the shear capacity computed according to Kowalsky and Priestley[36] with degradated parameters for steel and concrete evaluated as average values over the cross-section.

Analyses are stopped when either a failure criterion is met or the maximum experimental displacement is reached, according to which event occurs first.

7.2 | Influence of corrosion intensity

Guo et al.[37] tested rectangular sections reinforced at 1.6% with axial load ratio of about 10%. Deteriorated specimens where artificially corroded on the four sides up to 21.7% of the height with mass losses of about 5%, 10%, 15% (Figure A1). Figure 14 shows the comparison between experimental and numerical curves. For the test S1 neither 85% force reduction nor experimental failure was reported, therefore it was not possible to estimate the ultimate drift. Significant asymmetry is shown between the two loading directions. The discrepancies in the cyclic behavior are likely due to the occurrence of bar buckling and could be reduced by introducing low-cycle fatigue material. This fact does not influence the conclusions of the present validation which is focused on peak force and drift evaluated at 85% of the peak.

Rinaldi et al.[38] tested square sections reinforced at 0.9% with axial load ratio of about 16% (Figure A1). Deteriorated specimens where artificially corroded on the four sides up to 33.3% of the height with mass losses of about 25%. Two series of corroded–uncorroded tests were performed with different stirrups spacing, Figure 15 shows the results for the case with higher confinement, the other one is presented in Section 7.5.

Ma et al.[39] tested circular sections reinforced at 1.1% with variable axial load ratios (Figure A1). Deteriorated specimens where entirely corroded with mass losses of about 10%. Figure 16 shows the results for the tests with average axial load level and various corrosion intensities. The other ones from reference [39], characterized by different axial loads, are shown in Section 7.4. As before, the discrepancies in the cyclic behavior could be reduced

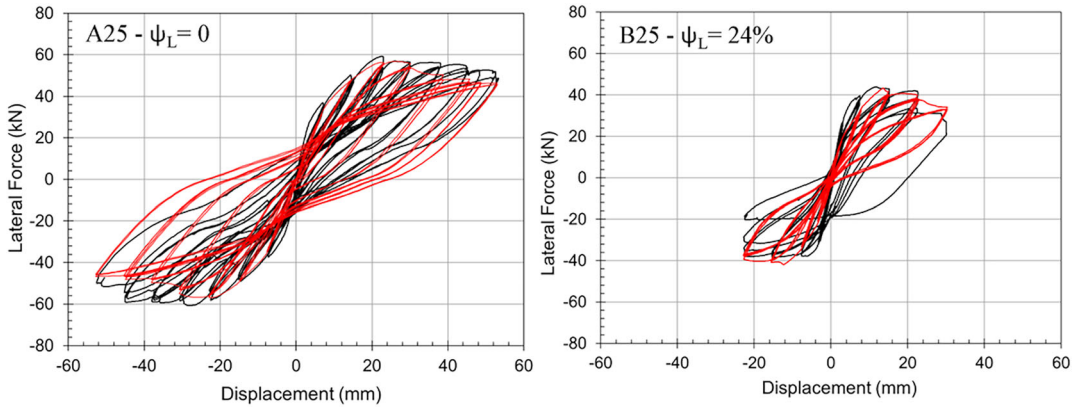

FIGURE 15 Tests A25–B25 from Rinaldi et al.[38] Mass loss shown in the plot corresponds to the measured average value.

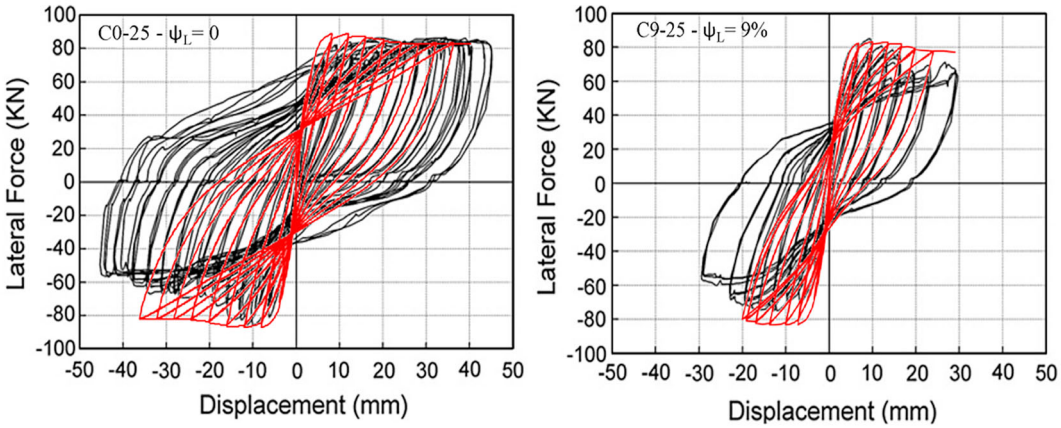

FIGURE 16 Tests C0-25, C9-25 from Ma et al.[39] with 25% axial load ratio. Mass loss shown in the plot corresponds to the measured average value.

TABLE 13 Influence of corrosion intensity evaluated in terms of ratios between the response of corroded and plain specimens.

				Corroded vs. uncorroded strength reduction			Corroded vs. uncorroded ultimate drift reduction		
	Specimen ID	**Reference**	ψ_L (%)	**Exp**	**Num**	**Err**	**Exp**	**Num**	**Err**
Guo et al.[37]	S2	S1	5	0.894	0.931	4.2%	-	-	-
	S3	S1	9.7	0.849	0.871	2.7%	-	-	-
	S4	S1	15.2	0.820	0.792	−3.4%	-	-	-
Rinaldi et al.[38]	B25	A25	23.7	0.743	0.764	2.9%	0.448	0.475	6.2%
	B30	A30	24.6	0.716	0.738	3.1%	0.499	0.533	6.9%
Ma et al.[39]	C9-15	C0-15	9	0.871	0.949	9.0%	1.104	0.869	−21.3%
	C9-25	C0-25	9	0.971	0.954	−1.7%	0.618	0.699	13.2%
	C9-40	C0-40	9	1.009	0.953	−5.6%	1.059	0.924	−12.8%
Average error						4.1%			12.1%

Note: Drift reduction ratios for Guo et al.[37] are absent since it was not possible to determine the ultimate drift of the reference test.

by modeling low-cycle fatigue and specific calibration of the cyclic parameters, but the fine-tuning of cyclic response is outside the scope of this work.

Table 13 summarizes the accuracy of the modeling in the prediction of the influence of corrosion on strength and ultimate drift by showing the ratios of the two

properties evaluated on corroded and uncorroded specimens. It turns out that the ratios are predicted with average errors of 4.1% and 12.1% respectively for strength and drift.

7.3 | Non-uniform sectional pattern

Lignola et al.[40] tested rectangular hollow sections with aspect ratio 1.5 reinforced at 0.9% with about 5% axial load (Figure A1). Deteriorated specimen was artificially corroded only on one of the shorter sides up to 40% of the height with mass loss of about 10%.

This is the only experimental case in which sectional corrosion pattern is non-uniform. Numerical simulations predict a lower flexural strength on the direction where corroded bars are in tension, but this effect is not evident in the experiments. However, asymmetry has been observed experimentally in the shear failure. Authors report shear failure at a drift of 2.74% on the negative side as opposed to 5.0% in the positive one. The numerical simulation, based on capacity model,[34] predicts, with very good approximation, a shear failure at a drift of 2.5% (Figure 17).

7.4 | Influence of axial load

Figure 18 shows two pairs of corroded–uncorroded tests from reference [39] carried out with axial load ratios of 15% and 40%, to be considered together with the analogous tests carried out at 25%, already reported in Figure 16.

Table 14 shows strengths and ultimate drifts with variable axial load ratios normalized with respect to those associated with the lower ALR. It turns out that ratios are predicted with average errors of 8.4% and 11.6% respectively for strength and drift.

7.5 | Influence of confinement

Figure 19 shows a pair of corroded–uncorroded tests from reference [38] to be compared with those in Figure 15. The two pairs are analogous except for the fact that those in Figure 19 have a lower confinement level.

Table 15 shows strengths and ultimate drifts with larger stirrups spacing normalized with respect to those obtained with the shorter one. It turns out that ratios are predicted with average errors of 1.3% and 0.6% respectively for strength and drift.

7.6 | Summary of the results

Table 16 summarizes the results of all simulations in terms of strength and ultimate drift for experimental and numerical tests. It turns out that the two quantities are predicted with an average error of 2.9% and 6.3%, respectively.

8 | CONCLUSIONS

The proposed practice-oriented modeling framework can be used for real RC structures subject to arbitrarily complex corrosion scenarios when information about deterioration is limited to qualitative judgments that can be formulated from in-situ survey.

The local deterioration scale for materials is based on the inversion of the degradation laws, so that the qualitative levels correspond to specific ranges of ASCE material properties reduction. New degradation laws for steel have been proposed on the basis of statistical evaluation of 17 existing laws based on a total of 898 samples.

The combined use of the global deterioration scale for zones and deterioration attenuation law allows one to

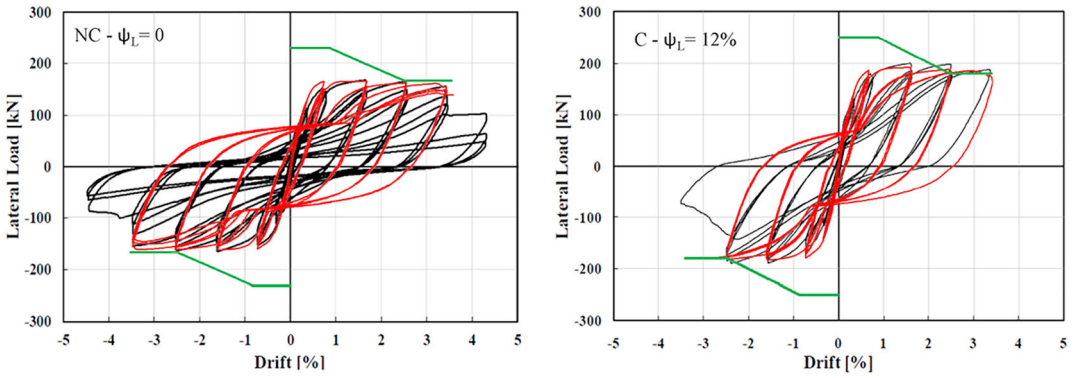

FIGURE 17 Tests NC (left) and C (right) from Lignola et al.[40] Mass loss shown in the plot corresponds to the measured average value. In green: shear capacity.

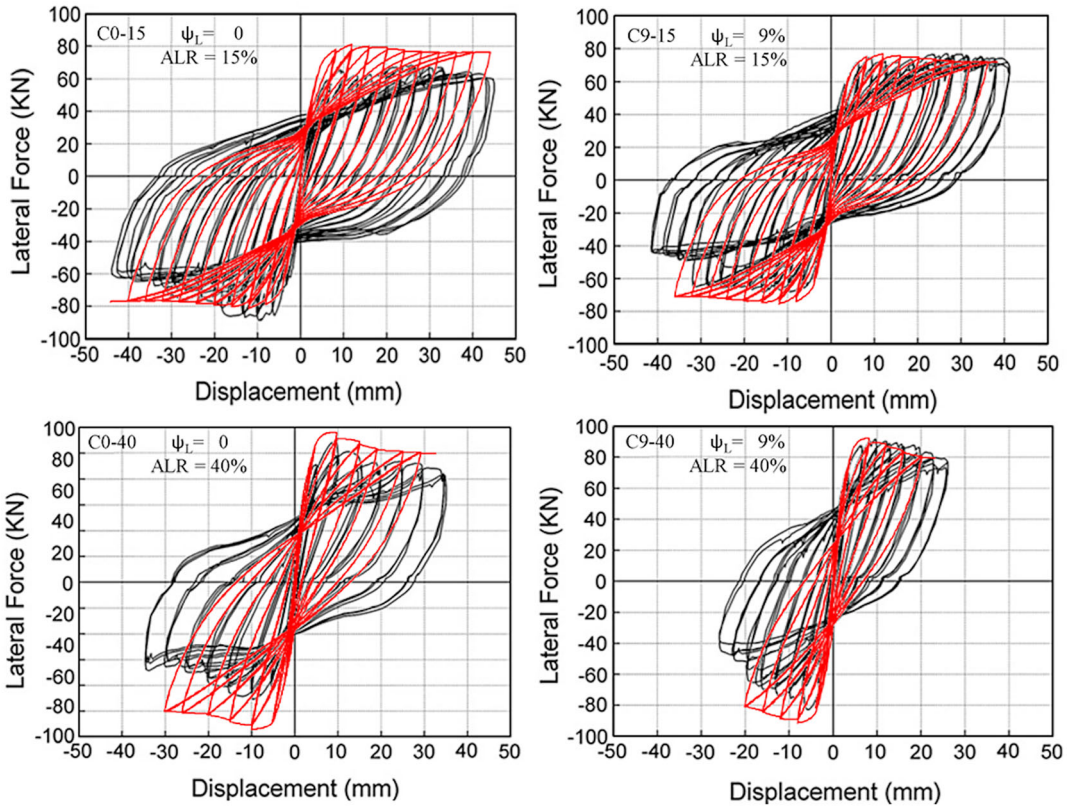

FIGURE 18 Corroded and uncorroded tests with ALR of 15% and 40% from Ma et al.[39]

TABLE 14 Influence of axial load evaluated in terms of ratios between the response of tests with higher and lower axial load.

				Higher vs. lower axial load strength ratio			Higher vs. lower axial load ultimate drift ratio		
Specimen ID	**Reference**	**Type**	**ALR (%)**	**Exp**	**Num**	**Err**	**Exp**	**Num**	**Err**
C0-25	C0-15	Plain	25–15	0.979	1.098	12.2%	1.209	1.000	−17.3%
C0-40	C0-15	Plain	40–15	1.020	1.203	18.0%	0.642	0.593	−7.7%
C9-25	C9-15	Corroded	25–15	1.091	1.104	1.2%	0.676	0.805	19.0%
C9-40	C9-15	Corroded	40–15	1.182	1.208	2.2%	0.616	0.630	2.3%
Average error						8.4%			11.6%

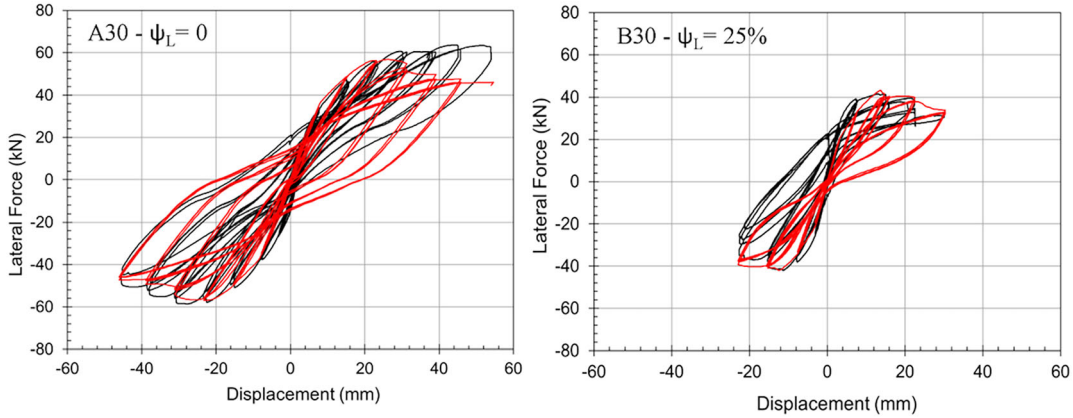

FIGURE 19 Tests A30, B30 from Rinaldi et al.[38]

TABLE 15 Influence of stirrups spacing evaluated in terms of ratios between the response of tests with higher and lower spacing.

				Lower vs. higher confinement strength ratio			Lower vs. higher confinement ultimate drift ratio		
Specimen ID	**Reference**	**Type**	**Stirrups spacing (cm)**	**Exp**	**Num**	**Err**	**Exp**	**Num**	**Err**
A30	A25	Plain	30–25	0.991	1.003	1.2%	0.859	0.851	−0.9%
B30	B25	Corroded	30–25	0.955	0.969	1.4%	0.957	0.955	−0.2%
Average error						1.3%			0.6%

TABLE 16 Summary of the results of the validation tests.

		F_p [kN]			$Drift_u$		
Source	**Specimen ID**	**Exp**	**Num**	**Error**	**Exp**	**Num**	**Error**
Rinaldi et al.[38]	A25	59.20	56.76	−4.1%	3.50%	3.37%	−3.8%
	B25	43.96	43.37	−1.4%	1.57%	1.60%	2.1%
	A30	58.67	56.92	−3.0%	3.01%	2.87%	−4.7%
	B30	42.00	42.03	0.1%	1.50%	1.53%	1.9%
Lignola et al.[40]	NC	163.35	161.76	−1.0%	3.70%	3.80%	2.7%
	C	190.81	182.34	−4.4%	2.74%	2.53%	−7.5%
Guo et al.[37]	S1	62.45	61.78	−1.1%	-	-	-
	S2	55.82	57.54	3.1%	3.97%	3.65%	−7.9%
	S3	53.00	53.84	1.6%	3.52%	3.30%	−6.2%
	S4	51.19	48.90	−4.5%	2.61%	2.78%	6.5%
Ma et al.[39]	C0-15	88.40	80.62	−8.8%	3.75%	4.42%	17.9%
	C9-15	76.98	76.48	−0.6%	4.14%	3.84%	−7.2%
	C0-25	86.50	88.52	2.3%	4.53%	4.42%	−2.5%
	C9-25	83.96	84.46	0.6%	2.80%	3.09%	10.4%
	C0-40	90.13	97.01	7.6%	2.41%	2.62%	8.8%
	C9-40	90.97	92.41	1.6%	2.55%	2.42%	−5.1%
Average error				2.9%			6.3%

model the penetration of the deterioration based on the specification of a qualitative judgment of the deterioration on the exposed surface.

In absence of more specific information, deterioration scales and attenuation law can be specified by plausible assumptions. However, further developments are currently ongoing to formulate more specific laws by means of detailed simulations of cracking patterns and diffusion analyses of corrosive agents.

The modeling framework has been implemented in OpenseesPy as a macroelement of arbitrarily corroded beam-column embedded in a Python application with full-fledged pre and post-processing that can be used to perform pushover analyses of single and multiple-columns piers as well as for framed structures.

The approach has been validated by comparison with 16 experimental tests modeled with material parameters determined by the proposed deterioration scales. Experiments have been selected to include a variety of different sections, reinforcement ratios, corrosion scenarios and confinement levels. Results showed an average accuracy of 2.9% on strength and 6.3% on ultimate drift. Specific investigations on the influence of corrosion intensity, axial load ratio, shear failure and stirrups spacing, similarly showed a remarkable agreement with experimental data.

ACKNOWLEDGEMENTS

We gratefully acknowledge the role of Italian Ministry for Infrastructures (MIMS) and ASPI, Autostrade per l'Italia S.p.a. in promoting and supporting project PRESIDEST from which this research originated. We sincerely thank Prof. Zila Rinaldi for sharing experimental data from reference [38].

DATA AVAILABILITY STATEMENT

Data sharing is not applicable to this article as no new data were created or analyzed in this study.

ORCID

Davide Bernardini https://orcid.org/0000-0002-3683-9831
Daniela Ruta https://orcid.org/0000-0002-2478-8934
Paolo Di Re https://orcid.org/0000-0002-3093-2728

REFERENCES

1. Ozbolt J, Balabanic G, Kuster M. 3D numerical modelling of steel corrosion in concrete structures. Corros Sci. 2011;53:4166–77.
2. Chauhan A, Desai Y, Banerjee S, Sharma UK. 3D simulation of non-uniform corrosion induced damage in reinforced concrete exposed to real climate. Structure. 2023;56:104852.
3. Kashani MM, Maddocks J, Dizaj EA. Residual capacity of corroded reinforced concrete bridge components; state-of-the-art review. J Bridge Eng. 2019;24(7):3119001_1–3119001_16.
4. Andisheh K, Scott A, Palermo A. Seismic behavior of corroded RC bridges: review and research gaps. Int J Corros. 2016;2016(3075184):1–22.
5. Imperatore S. Mechanical properties decay of corroded reinforcement in concrete – an overview. Corros Mater Degrad. 2022;3(2):210–20.
6. Bernardini D, Di Re P, Ruta D, Paolone A. Modeling non-uniform corrosion in reinforced concrete bridge piers. Lect Notes Civ Eng. 2021;200:372–9.
7. Bernardini D, Carbone G, Di Re P, La Morgia M, Mei A, Paolone A, et al. OpenSeesPy-based web application for pushover curve computation of RC bridge piers subject to arbitrarily non-uniform corrosion patterns. Lect Notes Civ Eng. 2023;326:86–96.
8. Bernardini D, Braga F, Buttarazzi F, Cardone D, Di Re P, Migliorino P, et al. Influence of spatially heterogeneous deterioration patterns on strength and ductility of corroded reinforced concrete bridge piers. Procedia Struct Integrity. 2023;44:649–56.
9. Liu J, Luo X, Chen Q. Degradation of steel rebar tensile properties affected by longitudinal non-uniform corrosion. Materials. 2023;16:2917.
10. Li D, Wei R, Xing F, Sui L, Zhou Y, Wang W. Influence of non-uniform corrosion of steel bars on the seismic behavior of reinforced concrete columns. Construct Build Mater. 2018;167:20–32.
11. Ou YC, Susanto YTT, Roh H. Tensile behavior of naturally and artificially corroded steel bars. Construct Build Mater. 2016;103:93–104.
12. Imperatore S, Rinaldi Z, Drago C. Degradation relationships for the mechanical properties of corroded steel rebars. Construct Build Mater. 2017;148:219–30.
13. Lee H-S, Cho Y-S. Evaluation of mechanical properties of steel reinforcement embedded in concrete specimen as a function of the degree of reinforcement corrosion. Int J Fract. 2009;157:81–8.
14. Lu C, Yuan S, Liu R. Mechanical properties of corroded steel bars in pre-cracked concrete suffering from chloride attack. Construct Build Mater. 2016;123:649–60.
15. Vanama RK, Ramakrishnan B. Improved degradation relations for the tensile properties of naturally and artificially corroded steel rebars. Construct Build Mater. 2020;249:118706.
16. Xia J, Jin W-L, Zhao Y-X, Li L-Y. Mechanical performance of corroded steel bars in concrete. Struct Build. 2013;166:235–46.
17. Zhang W, Song X, Gu X, Li S. Tensile and fatigue behavior of corroded rebars. Construct Build Mater. 2012;34:409–17.
18. Du YG, Clark LA, Chan AHC. Residual capacity of corroded reinforcing bars. Mag Concr Res. 2005;57(3):135–47.
19. Sun X, Kong H, Wang H, Zhang Z. Evaluation of corrosion characteristics and corrosion effects on the mechanical properties of reinforcing steel bars based on 3D scanning. Corros Sci. 2018;142:284–94.
20. Coronelli D, Gambarova P. Structural assessment of corroded reinforced concrete beams: modeling guidelines. J Struct Eng. 2004;130(8):1214–24.
21. Vidal T, Castel A, François R. Analyzing crack width to predict corrosion in reinforced concrete. Cem Concr Res. 2004;34:165–74.
22. Bossio A, Lignola GP, Fabbrocino F, Monetta T, Prota A, Bellucci F, et al. Nondestructive assessment of corrosion of reinforcing bars through surface concrete cracks. Struct Concr. 2017;18:104–17.
23. Kien D, Nenad G. Factors affecting the detectability of concrete delamination in GPR images. Construct Build Mater. 2021;274:121837.
24. Campione G, Cannella F, Minafò G. A simple model for the calculation of the axial load-carrying capacity of corroded RC columns. Mater Struct. 2016;49:1935–45.
25. Scott MH, Fenves GL. Plastic-hinge integration methods for force-based beam-column elements. ASCE J Struct Eng. 2006;132(2):244–52.
26. Scott MH, Hamutcuoglu OM. Numerically consistent regularization of force-based frame elements. Int J Numer Methods Eng. 2008;76:1612–31.
27. Kashani MM, Lowes LN, Crewe AJ, Alexander NA. Nonlinear fibre element modeling of RC bridge piers considering inelastic bucking of reinforcement. Eng Struct. 2016;116:163–77.
28. Krolicki J, Maffei J, Calvi GM. Shear strength of reinforced concrete walls subjected to cyclic loading. J Earthquake Eng. 2011;15:30–71.
29. Braga F, Gigliotti R, Laterza M, D'Amato M, Kunnath S. Modified steel bar model incorporating bond-slip for seismic assessment of concrete structures. J Struct Eng. 2012;138:1342–50.
30. Sezen H, Setzler EJ. Reinforcement slip in reinforced concrete columns. ACI Struct J. 2008;105:280–9.
31. Zhang Y, Bicici E, Sezen H, Zheng S. Reinforcement slip model considering corrosion effects. Construct Build Mater. 2020;235:117348.
32. LeBorgne MR, Ghannoum WM. Local deformation measures for RC column shear failures leading to collapse. ATC & SEI conference on improving the seismic performance of existing buildings and other structures, San Francisco, USA; 2009. Reston, VA: American Society of Civil Engineers.
33. Chen H, Li H-N, Biondini F, Wang D-S, Zou Y. Strain penetration effect on cyclic response of corroded RC columns. Eng Struct. 2021;243:112653.
34. Cassese P, Ricci P, Verderame GM. Experimental study on the seismic performance of existing reinforced concrete bridge piers with hollow rectangular section. Eng Struct. 2017;144:88–106.

35. Ranzo G, Priestley MJN. Seismic performance of large circular hollow columns. 12th world conference on earthquake engineering, Auckland, New Zealand; 2000. Auckland, New Zealand: Society for Earthquake Engineering.
36. Kowalsky MJ, Priestley MJN. Improved analytical model for shear strength of circular concrete columns in seismic regions. ACI Struct J. 2000;97(3):388–96.
37. Guo A, Li H, Guan X, Li H. Experimental investigation on the cyclic performance of RC piers with chloride-induced corrosion in marine environment. Eng Struct. 2015;105:1–11.
38. Rinaldi Z, Di Carlo F, Spagnuolo S, Meda A. Influence of localised corrosion on the cyclic response of RC columns. Eng Struct. 2022;256:114037.
39. Ma Y, Che Y, Gong J. Behavior of corrosion damaged circular RC columns under cyclic loading. Construct Build Mater. 2012; 29:548–56.
40. Lignola GP, Fabbrocino F, Prota A, Cosenza E, Manfredi G. Reinforcement corrosion in RC hollow piers: destructive and non-destructive tests. Materials. 2023;16:2790.

AUTHOR BIOGRAPHIES

Davide Bernardini, Department of Structural and Geotechnical Engineering, University of Rome Sapienza, Rome, Italy. Email: davide.bernardini@uniroma1.it.

Daniela Ruta, Department of Structural and Geotechnical Engineering, University of Rome Sapienza, Rome, Italy. Email: daniela.ruta@uniroma1.it.

Paolo Di Re, Department of Structural and Geotechnical Engineering, University of Rome Sapienza, Rome, Italy. Email: paolo.dire@uniroma1.it.

Achille Paolone, Department of Structural and Geotechnical Engineering, University of Rome Sapienza, Rome, Italy. Email: achille.paolone@uniroma1.it.

How to cite this article: Bernardini D, Ruta D, Di Re P, Paolone A. A fiber-based deterioration modeling framework for reinforced concrete structures subject to spatially non-uniform corrosion patterns described by limited information. Structural Concrete. 2025;26(5): 5650–76. https://doi.org/10.1002/suco.202400577

APPENDIX A

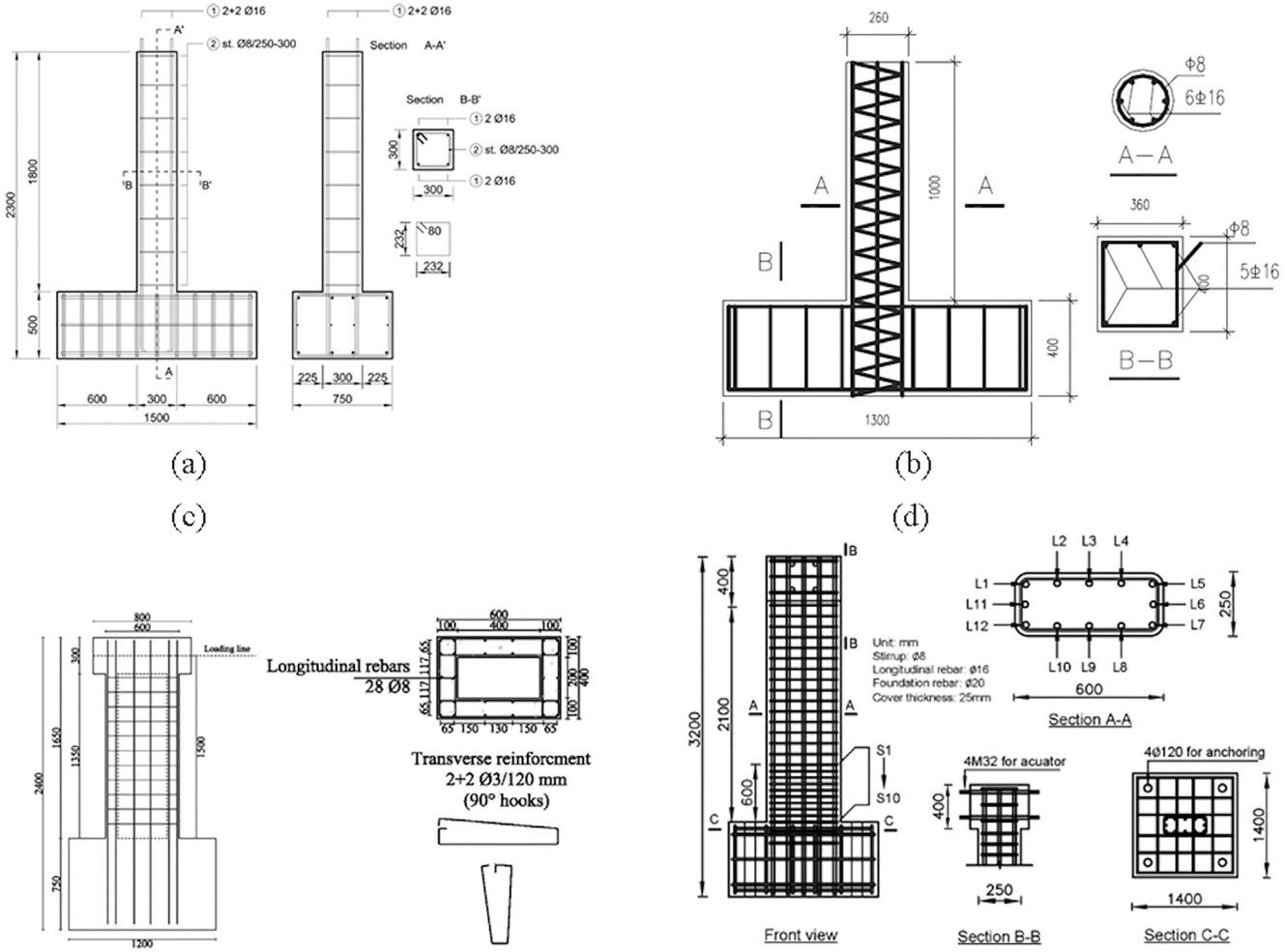

FIGURE A1 Description experimental tests: (a) Rinaldi et al.,[38] (b) Ma et al.,[39] (c) Lignola et al.,[40] (d) Guo et al.[37]